Chapter 7
Magnetophoresis in Bio-Devices

Anne-Laure Deman and Damien Le Roy

Abstract Associating magnetism to microfluidics is a powerful approach to address challenges in biomedical applications. Indeed, due to the versatility of this approach, it can be exploited in applications as diverse as blood fractionation and Circulating Tumor Cell separation and detection. The separation and manipulation of sub-mm particles, such as magnetically labelled biological cells, magnetic micro- and nano-particles, are achieved thanks to magnetophoresis forces arising from magnetic flux gradients, engineered inside of microfluidics devices. In this chapter, basic concepts to understand physical phenomena, to design and optimize magnetic bio-micro-devices are presented. Finally, few examples of such devices are given to illustrate the potential of this approach.

7.1 Introduction

In microdevices, magnetism can be used to realize valves, to achieve pumping functions, or the manipulation of micro- or nano-objects inside microfluidic channels. The objects responding to the magnetic field could be either particles or cells, using extrinsic or native magnetic properties. *Magnetophoresis*, which refers

A.-L. Deman (✉)
Institut des Nanotechnologies de Lyon (INL), CNRS, UMR 5270,
Université de Lyon 1, Université de Lyon, Villeurbanne 69622, France
e-mail: anne-laure.deman-him@univ-lyon1.fr

D. Le Roy
Campus LyonTech La Doua, Université Lyon 1 et Institut Lumière Matière,
10, Rue Ada Byron, Villeurbanne 69622, France
e-mail: damien.le-roy@univ-lyon1.fr

to the motion of an object in a non-uniform magnetic field, permits to address numerous biomedical issues. Indeed, micro-and nano-particles can be functionalized by multiple coating, proteins, or molecules offering multifunctionality, and magnetic labelling of cells can be obtained using specific cell biomarkers. By mastering microfluidic designs, magnetic field gradients can be patterned to optimize targeting and controllability. Moreover, magnetic interactions offer contactless manipulation, thus preserving biological entities, and do not depend, or in a negligible way, on the pH or the conductivity of the medium, and can be designed to operate over a wide range of temperature. In addition, congestion surrounding microfluidic device is limited, as the magnetic approach can be implemented with permanent magnets, and so do not necessarily require external source of energy. In this chapter, we will first underline some magnetism principles that serve to describe magnetophoresis. We will then highlight all forces involved in microfluidic devices. In a third part, we will focus on the specificities that come with the implementation of magnetophoresis in microdevices, in particular the fabrication and integration of magnetic micropatterns. We will finish this chapter with some examples of bio-analysis performed using magnetophoretic devices.

7.2 Magnetism Principles for Magnetophoresis

To start addressing the question of *magnetophoresis*, which refers to the motion of an object in a non-uniform magnetic field, we will briefly recall some magnetostatic principles and apply them to the use of magnetic forces in microsystems. We will place the discussion in the context of an interaction between three elements: (1) a point-like magnetic dipole that is the object to manipulate, (2) a source of local variation of magnetic field that is the remote and (3) and an external magnetic field to assist the remote control. We focus our attention on static and quasi-static magnetic interactions, thus considering that the magnetic moment of the target object is aligned with the magnetic field it is submitted to.

7.2.1 Origin of the Magnetophoretic Force: A Magnetic Particle in an External Magnetic Field

The magnetic particle is described here by its magnetic moment $\vec{m}$. According to Ampère, a magnetic moment is equivalent to a tiny current loop. If the circulating current is I (in A), and if $\vec{S}$ is the oriented surface, then:

$$\vec{m} = I\,\vec{S} \tag{7.1}$$

provided that the current flows in a plane. The direction of $\overrightarrow{m}$ is given by the right-hand corkscrew rule.

To discuss the interaction between a magnetic moment and an external magnetic field, it is then convenient to describe the magnetic moment as its equivalent current loop and to consider the Laplace force $\overrightarrow{F_{L}}$ acting on it when submitted to a magnetic induction $\overrightarrow{B}$. The expression of $\overrightarrow{F_{L}}$ acting on a current loop of length ℓ, with circulating I and submitted to a magnetic induction $\overrightarrow{B}$ (in free space: $\overrightarrow{B} = \mu_0$ $\overrightarrow{H}$, and more generally one writes: $\overrightarrow{B} = \mu_r \, \mu_0 \, \overrightarrow{H}$, μ_r the relative dimensionless permeability of the medium), is:

$$\overrightarrow{F_{L}} = I \oint \overrightarrow{d\ell} \times \overrightarrow{B} \tag{7.2}$$

By calculating the moment of the Laplace force, one can show that a magnetic field $\overrightarrow{H}$, creates a torque $\overrightarrow{\Gamma}$ on a magnetic moment $\overrightarrow{m}$, expressed as:

$$\overrightarrow{\Gamma} = \overrightarrow{m} \times \overrightarrow{B} \tag{7.3}$$

This first result shows that when submitted to an external field, a magnetic moment will tend to align parallel to the field.

The '*potential energy*' of a magnetic moment in a field, also known as the *Zeeman energy*, E_Z, that is, apart from a constant:

$$E_Z = -\overrightarrow{m} \cdot \overrightarrow{B} \tag{7.4}$$

When a magnetic moment is in a uniform external field, there is a torque but no translational force. In contrast, if the external field is not uniform, the potential energy will depend on the position and this will lead to a net force that can be expressed as:
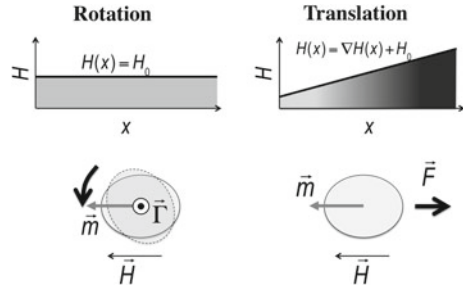
$$\overrightarrow{F} = -\overrightarrow{\nabla}E = \overrightarrow{\nabla}\left(\overrightarrow{m} \cdot \overrightarrow{B}\right) = \mu_r\mu_0\overrightarrow{\nabla}\left(\overrightarrow{m} \cdot \overrightarrow{H}\right) \tag{7.5}$$

This develops in:

$$\overrightarrow{F} = \mu_r\mu_0\left(\left(\overrightarrow{m} \cdot \overrightarrow{\nabla}\right)\overrightarrow{H} + \left(\overrightarrow{H} \cdot \overrightarrow{\nabla}\right)\overrightarrow{m} + \overrightarrow{m} \times \left(\overrightarrow{\nabla} \times \overrightarrow{H}\right) + \overrightarrow{H} \times \left(\overrightarrow{\nabla} \times \overrightarrow{m}\right)\right) \tag{7.6}$$

As there is no induced current in the particles, the third and fourth terms vanish (from Ampere's law) and assuming that the particle as a constant moment (which is

Fig. 7.1 Action of a
magnetic field on a magnetic
particle

the case for superparamagnetic particles), the second term can be neglected, which
reduces (7.6) to:

$$\overrightarrow{F} = \mu_0(\overrightarrow{m} \cdot \overrightarrow{\nabla})\overrightarrow{H} \tag{7.7}$$

This expression of the translational force shows that (i) it is non-zero only in
non-uniform magnetic field, and (ii) if the magnetic moment is parallel (/antipar-
allel) to the magnetic field then it will be attracted to the region of maximum
(/minimum) field, as illustrated in Fig. 7.1.

7.2.2 Role of the Magnetic Nature of the Object to Manipulate

Magnetophoresis is implemented in microfluidic systems to manipulate, sort, and
trap magnetic micro- or nano-objects, mainly. These objects are mainly: magnetic
micro- or nano-particles [1–3], magnetically labeled cells [4–6] or natively para-
magnetic cells such as deoxygenated Red Blood Cells (RBC) [7–9]. The magnetic
susceptibility establishes the relationship between H and the magnetization M (the
volume fraction of m), as $M = \chi H$. Based on this, micro- and nano-objects can be
divided into four different categories: diamagnetic, paramagnetic, ferromagnetic, or
superparamagnetic substances. The magnetic response of those materials to an
applied field is schematized in Fig. 7.2.

7.2.2.1 Diamagnets

A diamagnet is a substance composed of atoms that do not have any net magnetic
moment. This is usually the case of atoms with closed-shell electronic structures,
either monoatomic rare gases, model ionic solids like NaCl, or covalent solids like
diamond, silicon or germanium. Superconductors are perfect diamagnets, with a
magnetic susceptibility of −1. When subjected to an applied magnetic field, the
diamagnetic substance develops a negative moment, proportional to the field.

Fig. 7.2 Magnetic response of substances to a magnetic field as a function of their magnetic nature
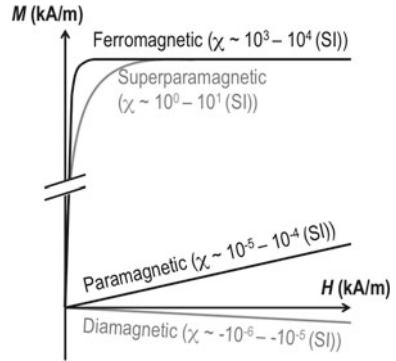
The theory of diamagnetism, initiated by Paul Langevin in early 20th century, considers that the applied field reduces the effective current of the electron orbits, which results in a magnetic moment that is opposite to the applied field.

In diamagnetic substances, the susceptibility does not vary with temperature (values of dimensionless volumetric magnetic susceptibility χ (SI) of various diamagnetic substances, fluids and solids, are reported in Table 7.1). Note that a superconductor is a perfect diamagnet with a susceptibility of -1. According to the above discussion, the experienced magnetic force thus scales with $-\nabla H^2$. Diamagnetic substances are therefore repelled from the regions of maximum magnetic field.

In general, organic matter is diamagnetic, and animal bodies have therefore an effective diamagnetic behavior. If the repelling force compensates for gravity, levitation can happen, as demonstrated in the experiment of A. Geim and M. Berry who made a frog fly over a superconducting coil. They received for it the Ig Nobel price in 2000.

Table 7.1 Dimensionless susceptibility χ of some substances at room temperature (Unit: 10^{-6} [SI]) [8–12]

Substance	χ (unit 10^{-6} [SI])
Water	-9.03
Bovine Serum Albumin (BSA)	-10.38
Blood plasma	-7.7
Ethanol	-7.28
Acetone	-5.78
WBC	-0.13
RBC in air (in H_2O)—oxyHb	-9.21 (-0.18)
RBC in air (in H_2O)—deoxyHb	-5.70 (3.33)
RBC in air (in H_2O)—met	-5.25 (3.78)
Cu	-22
Bi	-166
HOPG (//)	-450

Although diamagnets are generally considered insensitive to magnetic fields gradients as their intrinsic magnetic susceptibility are the smallest of all materials, significant response can be obtained by adjusting the magnetic susceptibility contrast between the diamagnetic object and its surrounding medium. For instance, in microfluidic devices, the medium can be doped with paramagnetic substances.

7.2.2.2 Paramagnets

In the same report on the theory of diamagnetism published in 1905, Paul Langevin addressed the dependence of paramagnet susceptibilities on the temperature (T) in $1/T$, measured by Pierre Curie in the late 19th century. Its generalization led to the so-called Curie-Weiss equation that establishes the relation between the magnetic susceptibility, χ, and the temperature as:

$$\chi = \frac{C'}{T - \theta} \tag{7.8}$$

with C' a constant, and θ a parameter that depends on the material.

In his simple description, Langevin assumed that the atoms in the material exhibit a net magnetic moment, which results from the fact that all spins and orbital moments of an atom do not cancel out. The atomic magnetic moments, hold by the unpaired electrons, do not interact with each other. In the absence of external magnetic field, the moments point in random directions, globally compensating for each other. Therefore, there is no net magnetization. When a magnetic field is applied, the moments tend to align with the field, but the thermal fluctuation impedes the alignment. Therefore, paramagnet present relatively small magnetic susceptibility that decays with the increase of temperature. From this description, if μ_{at} represents the atomic moment (here we assume they are all the same), the magnetization M of the paramagnet is given by the so-called Langevin function that is:

$$M = M_0 \left[coth\left(\frac{\mu_0 \mu_{at} H}{k_B T}\right) - \frac{k_B T}{\mu_0 \mu_{at} H} \right] \tag{7.9}$$

where M_0 is the maximum magnetization that the paramagnet can reach (all the magnetic moments are aligned with the applied field).

M_0 is the product of the volume density of atoms n (in m^{-3}) and the atomic moment $\mu_{at}(M_0 = n\mu_{at})$, H the applied field, k_B the Boltzmann constant.

When expressed as a series, the Langevin function first term leads to:

$$M = M_0 \frac{\mu_0 \mu_{at} H}{3 k_B T} \tag{7.10}$$

Table 7.2 Dimensionless susceptibility χ of some substances at room temperature (Unit: 10^{-6} [SI]) [13, 14]

Substance	χ (Unit: 10^{-6} [SI])
Al	20
Ca	22
Mg	12
Pd	805
Gd	476300

So the magnetic susceptibility $\chi = \frac{M}{H}$ is:

$$\chi = M_0 \frac{\mu_0 \mu_{at}}{3k_B T} \tag{7.11}$$

Table 7.2 gives the magnetic susceptibility of some paramagnets.

Considering that μ_{at} is only few μ_B (μ_B the Bohr magneton, 9.274 10^{-24} A·m^2), this result shows that a huge value of magnetic field, of the order of 10^5–10^6 kA·m^{-1} would be needed to reach M_0, which is possible experimentally.

7.2.2.3   Ferromagnets and Ferrimagnets

To describe ferromagnets and ferrimagnets, Weiss introduced in 1907 the notion of *molecular field,* which accounts for interactions between all individual atomic moments, and is proportional to the magnetization. This field does not exist in reality but it is a convenient way to approximate the effect of interactions between atomic moments, which is described in quantum mechanics by the Heisenberg Hamiltonian. In the case of ferromagnets, two adjacent magnetic moments are coupled parallel while in ferrimagnets there exists two sublattices holding different magnetic moments and coupled antiparallel. The strength of the interaction between two adjacent moments is characterized by the exchange stiffness A. Values of A for some ferromagnetic substances are reported in Table 7.3. The characteristic of ferromagnets (and ferrimagnets) is its spontaneous magnetization M_S, which represents the alignment of magnetic moments located on a crystal lattice. In the absence of magnetic field, the moments tend to align on preferential directions. The associated magnetic energy landscape that determines the orientation of the magnetization in the absence of any applied magnetic field is the magnetic anisotropy energy. Above a critical temperature that is named the Curie point, the magnetic order is abruptly reduced and the substance becomes a paramagnet. The Curie temperature can be as high as 1400 K (cobalt). It scales with the abovementioned exchange stiffness A. Apart from the spontaneous magnetization, ferromagnets are characterized by their structure in magnetic domains, already suggested by Weiss as an explanation for the absence of any remanent magnetization in a large fraction of ferromagnetic substances like iron. The domain structure results from a compromise between the exchange interactions between adjacent atomic moments that tends to

Table 7.3 Characteristic parameters of some ferromagnets [13, 15, 16]

Material	M_S (kA/m)	K_1 (kJ/m^3)	A (pJ/m)
Fe	1710	48	21
Co	1440	410	31
Ni	488	−5	8
$Ni_{80}Fe_{20}$	840	0.15	10
Fe_3O_4 (magnetite)	480	−13	7
γ-Fe_2O_3 (maghemite)	400	4.6	(10)
CoPt	810	4900	10
$SmCo_5$	860	17200	12
$Nd_2Fe_{14}B$	1280	4900	8

align them collinearly, the minimization of a self-energy term, also referred as magnetostatic energy, due to the dipole field that is created by the magnetization, and the anisotropy. Inside a ferromagnetic (or a ferrimagnetic) substance, the dipole field is named demagnetizing field, as it points in the opposite direction with respect to the magnetization.

In magnetically-hard compounds, the magnetic anisotropy energy is large enough to dominates over the magnetostatic energy term and the magnetic domains can remain significantly uncompensated when the applied field is removed. The net magnetization when the field is brought to zero is called the remanent magnetization (M_R). The applied field needed to bring the net magnetization to zero is called the coercive field. In contrast, the magnetic domains are compensated in magnetically-soft substances in which the anisotropy term is relatively small. Figure 7.3 shows characteristic magnetization curves for hard and soft ferromagnets. M_R and H_C are the remanent magnetization and the coercive field, respectively.

In most cases, the anisotropy originates from the crystalline structure. A high degree of symmetry, like in cubic lattices, leads to magnetic softness while a lower degree of symmetry, like hexagonal and tetragonal lattices leads to magnetic
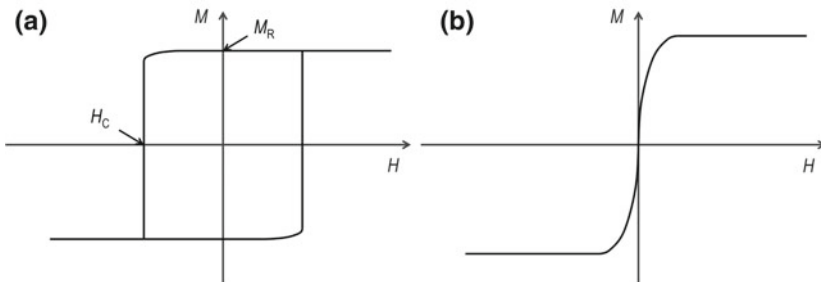
Fig. 7.3 Characteristic magnetization curves for hard **a** and soft **b** ferromagnets

hardness. The uniaxial term of the anisotropy energy density can be written as $K_1\sin^2\alpha$ with α the angle between the magnetization and its easy axis and K_1 the uniaxial anisotropy constant (in J/m^3) (see Table 7.3).

The magnetic response of soft ferromagnets to an applied field depends on its shape, through its demagnetizing tensor. In general, the demagnetizing field is not uniform within the volume of the ferromagnetic substance, except in ellipsoid shapes. Approximating the shape to an ellipsoid permits to predict the magnetic response to an applied field as the susceptibility is given by the simple following expression:

$$\chi = \frac{\chi_0}{1 + N\chi_0} \tag{7.12}$$

where N is a shape-dependent parameter called the demagnetizing factor (with values between 0 and 1), χ_0 the intrinsic magnetic susceptibility (related to the relative dimensionless magnetic permeability of the material, μ_r, by $\chi_0 = \mu_r - 1$).

The way to estimate the demagnetizing factor is discussed in the following (Sect. 7.3.3) in the context of the integration of magnetic flux concentrators.

In the case of objects of spherical shape, like for magnetic particles, the demagnetizing factor is equal to 1/3.

7.2.2.4 Superparamagnetism

The magnetic structure of nano-sized ferromagnets is usually single domain. Below a certain critical size, the energy cost of creating a domain wall is higher than the cost of magnetostatic energy. A well-established picture considers that all the magnetic moments of the object rotate coherently, and so add up to form giant magnetic moments, called macrospin. This model, known as the Stoner-Wohlfarth model, was proposed by two theoretical physicists, Edmund Clifton Stoner and Erich Peter Wohlfarth, in 1948. Note that if this model can well describe the magnetization reversal in the smallest size, it is often observed that before the magnetic structure breaks into multi-domain, the system loses the coherent rotation leading to other mechanism like curling reversal. It is also often observed that the anisotropy has a dominant uniaxial symmetry term, which can be originated from slightly elongated shape. Thus, a simple but commonly encountered model used to describe nano-sized ferromagnet is a macrospin with its magnetic anisotropy energy having two minima at 180° from each other. This is represented in Fig. 7.4.

The anisotropy energy barrier separating two minima can be expressed as the product of an effective anisotropy constant K_{eff} (in J/m^3) and the volume of the object V. In the bulk, the anisotropy constant K_1 varies over a wide range, it is of the order of 1–10 kJ/m^3 for relatively soft ferromagnets and 10^3–10^4 kJ/m^3 for hard ferromagnets. When a field is applied, the energy barrier becomes asymmetric, one of the two energy wells is the favored compared to the other and thus the energy

Fig. 7.4 Magnetic anisotropy energy profile for a macrospin with uniaxial anisotropy, as a function of the angle that the macrospin makes with the easy axis, denoted α
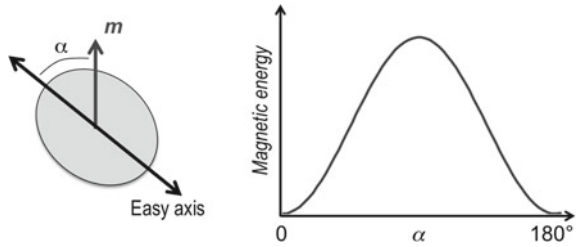
barrier is reduced. Néel proposed that the macrospin would flip its orientation at a time that follows an Arrhenius law:

$$\tau = \tau_0 exp\left(\frac{K_{eff}V}{k_B T}\right) \tag{7.13}$$

$1/\tau_0$ is the attempt frequency, typically of the order of 1 GHz, which is the ferromagnetic resonance frequency in the demagnetizing field. There is a continuous variation of the relaxation time with temperature. Assuming a measurement time of about 100 s in magnetometers, a commonly used figure of merit is the so called blocking temperature, that corresponds to the temperature for which: $K_{eff}V = 25$ $k_B T$. Figure 7.5 displays the temperature dependence of the relaxation times for Fe nanoparticles.

Table 7.4 gives the uniaxial term of the anisotropy for benchmark ferromagnets and some critical sizes: D_{coh} is the maximum particle diameter for coherent rotation and D_{sp} is the maximum diameter for «stable» magnetization direction.

l_{ex} reflects the compromise between the exchange energy that align two adjacent magnetic moments and the magnetostatic energy.

Fig. 7.5 Temperature dependence of the Néel relaxation time of Fe nanoparticles with diameters of 5, 10, and 15 nm
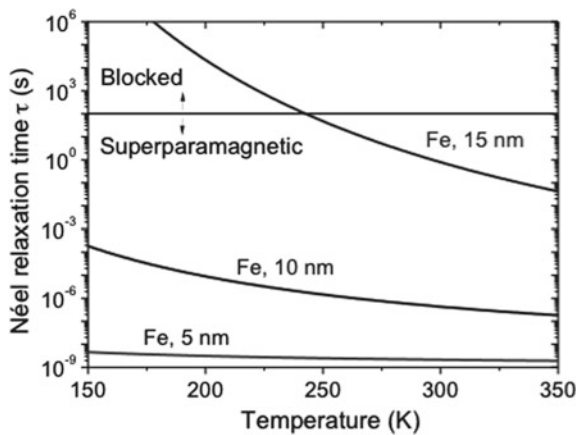
Table 7.4 Characteristic parameters and lengths in some ferromagnets [13]

Material	M_S (kA/m)	K_1 (kJ/m^3)	l_{ex} (nm) $l_{ex} = \sqrt{\frac{A}{\mu_0 M_S^2}}$	D_{coh} (nm) $D_{coh} = 2\sqrt{24}l_{ex}$	D_{sp} (nm) $D_{sp} \approx \sqrt{\frac{50 k_B T}{K_1}}$
Fe	1710	48	2.4	24	16
Co	1440	410	3.4	34	8
Ni	488	−5	5.1	50	34
Fe$_3$O$_4$	480	−13	4.9	48	26
CoPt	810	4900	3.5	34	3.4
SmCo$_5$	860	17200	3.6	36	2.2
Nd$_2$Fe$_{14}$B	1280	4900	1.9	19.4	3.4

Far from the blocking state (i.e. for measuring time greater than the Néel relaxation time), an ensemble of non-interacting macrospins in the superparamagnetic state responds to an applied field as a paramagnet with giant elementary moments, typically in the order of 10^2 to 10^4 μ_B, while it is of the order of few μ_B in paramagnet. As a consequence, there is no remanence magnetization and the magnetization curve is similar to the one reported in Fig. 7.3b. Therefore, one can describe the system magnetization with a Langevin function of the form:

$$M = M_0 \left[\coth\left(\frac{M_S V_P H}{k_B T}\right) - \frac{k_B T}{M_S V_P H} \right] \tag{7.14}$$

where V_P is the volume of the particle, M_S its spontaneous magnetization and M_0 the magnetization of the particle ensemble.

At relative low field, the magnetization of the ensemble varies linearly with the applied field, and the susceptibility is:

$$\chi = \frac{\mu_0 n (M_S V_P)^2}{3 k_B T} \tag{7.15}$$

where n is the volume density of particles.

As compared to paramagnetic substances, the field needed to reach saturation is relatively low, of the order of 10^1–10^2 kA/m. When the applied field is greater than this critical value, the magnetization of the particle saturates and the susceptibility can then be expressed as:

$$\chi = \frac{n M_S V_P}{H} \tag{7.16}$$

Most of the objects that are manipulated in microfluidic devices are superparamagnetic. They can be either individual nanoparticles or composites particles that are composed of nanoparticles embedded in a non-magnetic matrix.

7.3   Magnetic Micro- or Nano-Object Transport in Magnetophoretic System

In this section, we describe forces experienced by micro- or nano-object in microfluidic channel, during magnetophoresis experiments. For the sake of readability, we will describe forces in presence, one by one, considering a model magnetic particle (i.e. homogeneous and isotropic shape and magnetic properties).

Magnetic particles are submitted to various forces when flowing in a micro-channel [17–19]: (1) magnetophoretic force due to magnetic field gradients $\overrightarrow{F_{\mathrm{m}}}$, (2) fluidic drag force $\overrightarrow{F_{\mathbf{d}}}$, (3) gravitational force $\overrightarrow{F_{\mathrm{g}}}$, (4) buoyance forces $\overrightarrow{F_{\mathrm{b}}}$, (5) thermal kinetic energy (Brownian motion), and finally (6) forces resulting from inter-particle interactions, interactions between particles and micro-channel walls and interactions between particles and fluid. Analyzing the forces balance is required to anticipate particles motion in micro-channels in order to design sorting and trapping magnetic functions.

7.3.1   Magnetophoretic Force

Considering a particle of volume V_p and magnetization M_p, the magnetophoretic force in free space, can be expressed as follow based on Eq. (7.7):

$$\overrightarrow{F_{\mathrm{m}}} = \mu_0 \left(\overrightarrow{m} \cdot \overrightarrow{\nabla} \right) \overrightarrow{H} = \mu_0 V_p \left(\overrightarrow{M}_p \cdot \overrightarrow{\nabla} \right) \overrightarrow{H} \qquad (7.17)$$

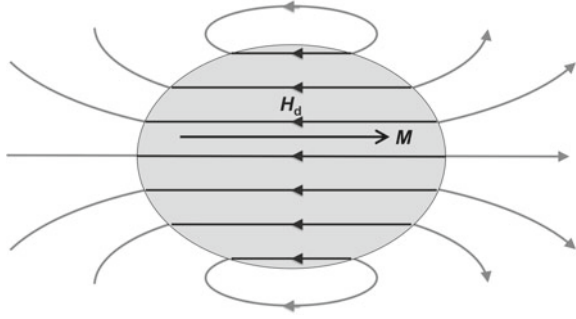The particle magnetization is expressed as:

$$\overrightarrow{M}_p = f(H) \overrightarrow{H} \qquad (7.18)$$

where $f(H)$ is a function of which expression depends on whether the particle magnetization is saturated or not, i.e. on the magnitude of the magnetic field.

At low magnetic field, the particle magnetization is not saturated and the magnetization varies linearly with the applied field and so $f(H) = \chi_m$, χ_m being the measured magnetic susceptibility.

As mentioned in the section introducing ferromagnets, the internal magnetic field in magnetic objects, $\overrightarrow{H_{\mathrm{int}}}$, differs from the external field, $\overrightarrow{H}$, by a quantity that scales with the magnetization. Thus, at a given position in the volume: $\overrightarrow{H_{\mathrm{int}}} = \overrightarrow{H} + \overrightarrow{H_{\mathrm{d}}}$, with $\overrightarrow{H_{\mathrm{d}}}$ the so-called demagnetizing field, that is opposed to the magnetization that creates it, as schematized in Fig. 7.6. Therefore, one should distinguish the intrinsic susceptibility $\chi_0 (\vec{M}_p = \chi_0 \overrightarrow{H_{\mathrm{int}}})$ from the measured susceptibility, $\chi_m (\vec{M}_p = \chi_m \vec{H})$.

Fig. 7.6 Schematics of the field created inside and outside a uniformly magnetized ellipsoid object. It is generally referred inside as the demagnetizing field, and outside as the dipolar field

As a result, the magnetization can be expressed as:

$$\overrightarrow{M}_P = \chi_m \overrightarrow{H} = \frac{\chi_0}{1+N\chi_0}\overrightarrow{H} \tag{7.19}$$

For spherical particles where $N = 1/3$, Eq. (7.19) becomes:

$$\overrightarrow{M}_P = \chi_m \overrightarrow{H} = \frac{3\chi_0}{3+\chi_0}\overrightarrow{H} \tag{7.20}$$

In a microfluidic device, the micro-particle is immersed in a fluid of magnetic susceptibility χ_f, and magnetic permeability μ_f. As described by Furlani et al. [20] the expression of the force on a magnetized particle is then:

$$\overrightarrow{F}_m = \mu_f V_p \frac{3(\chi_0 - \chi_f)}{(\chi_0 - \chi_f)+3(1+\chi_f)}\left(\overrightarrow{H}\cdot\overrightarrow{\nabla}\right)\overrightarrow{H} \tag{7.21}$$

For large magnetic fields, the particle magnetization is saturated (all atomic moments being aligned along the magnetic field) and $\overrightarrow{M}_p = \overrightarrow{M}_{sp}, \left|\overrightarrow{M}_{sp}\right| = M_{sp}$ being the magnetization at saturation.

As a consequence, depending on the magnetic field, when $\mu_f \approx \mu_0$ $(|\chi_f| \ll 1)$, $\overrightarrow{F}_m$ can be expressed as follow:

$$\vec{F}_m = \begin{cases} \mu_0 V_p \frac{3(\chi_0-\chi_f)}{(\chi_0-\chi_f)+3}\left(\vec{H}\cdot\overrightarrow{\nabla}\right)\vec{H}, & H < \left(\frac{(\chi_0-\chi_f)+3}{3(\chi_0-\chi_f)}\right)M_{sp}, \\ \mu_0 V_p \left(\overrightarrow{M}_{sp}\cdot\overrightarrow{\nabla}\right)\vec{H}, & H \geq \left(\frac{(\chi_0-\chi_f)+3}{3(\chi_0-\chi_f)}\right)M_{sp}, \end{cases} \tag{7.22}$$

For micro- or- nano-particles, depending on their magnetic properties, the expression of $\overrightarrow{F}_m$ becomes:

$$\chi_0 <\, <1, \vec{F}_m = \begin{cases} \mu_0 V_p \left(\chi_0 - \chi_f \right) \left(\vec{H} \cdot \vec{\nabla} \right) \vec{H}, & H < \frac{M_{sp}}{\chi_0 - \chi_f}, \\ \mu_0 V_p \left(\vec{M}_{sp} \cdot \vec{\nabla} \right) \vec{H}, & H \geq \frac{M_{sp}}{\chi_0 - \chi_f}, \end{cases} \tag{7.23}$$

$$\chi_0 >\, > 1, \vec{F}_m = \begin{cases} \mu_0 V_p 3 \left(\vec{H} \cdot \vec{\nabla} \right) \vec{H}, & H < \frac{M_{sp}}{3}, \\ \mu_0 V_p \left(\vec{M}_{sp} \cdot \vec{\nabla} \right) \vec{H}, & H \geq \frac{M_{sp}}{3}, \end{cases} \tag{7.24}$$

Equation (7.23) shows that the particle will be subjected either to a positive force in the case of $\chi_0 > \chi_f$ or to a negative force, if $\chi_f > \chi_0$, and then either attracted or repelled from maximum of magnetic field gradient [21]. These motions refer to positive and negative magnetophoresis [22].

To summarize, when magnetophoresis is implemented in microfluidic devices, particles magnetization can be saturated or not based on its own magnetic properties and on the magnitude of the applied magnetic field. As a result, the magnetophoretic force can be either proportional to $\left(\vec{H} \cdot \vec{\nabla} \right) \vec{H}$ or to $\vec{\nabla} \vec{H}$, as reported in Table 7.5.

The size of the object, its magnetic properties, as well as the magnetic field and its gradient are key parameters to improve magnetophoretic forces. In microfluidic devices, magnetophoretic forces reported in literature ranges from few pN to several nN, depending on the objects and magnetic system implemented (see Sect. 7.3).

7.3.2 Fluidic Drag Force

Viscous drag force acts on particle in the opposite direction to their motion. In low Reynolds fluid flow conditions, the drag force is expressed using Stokes' law, as follow [1]:

$$\vec{F}_d = 6\pi\eta R_p \left(\vec{v}_f - \vec{v}_p \right) f_D \tag{7.25}$$

where R_p is the radius of the particle, $\vec{v}_p$ its the velocity, η and $\vec{v}_f$ respectively the viscosity of the external medium and the velocity of the fluid. f_D is the drag

Table 7.5 Expression of magnetophoretic force depending on the magnitude of the magnetic field and on the magnetic susceptibility of the particle $\left(\Delta\chi = \left(\chi_0 - \chi_f \right) \right)$

Non-saturated particles (low magnetic field)		Saturated particles (large magnetic field)
$\chi_0 \ll 1$	$\chi_0 \gg 1$	
$\vec{F}_m = \mu_0 V_p \Delta\chi \left(\vec{H} \cdot \vec{\nabla} \right) \vec{H}$	$\vec{F}_m = \mu_0 V_p 3 \left(\vec{H} \cdot \vec{\nabla} \right) \vec{H}$	$\vec{F}_m = \mu_0 V_p \left(\vec{M}_{sp} \cdot \vec{\nabla} \right) \vec{H}$

coefficient of the particle that takes into account the influence of a solid wall in the vicinity of the particle, z being the distance of the particle to the wall [1, 19].

$$f_D = \left[1 - \frac{9}{16}\left(\frac{R_p}{R_p + z}\right) + \frac{1}{8}\left(\frac{R_p}{R_p + z}\right)^3 - \frac{45}{256}\left(\frac{R_p}{R_p + z}\right)^4 - \frac{1}{16}\left(\frac{R_p}{R_p + z}\right)^5\right]^{-1}$$

(7.26)

f_D varies between 1, for particle distant from the wall to 3 for particle in contact with micro-channel wall ($z = 0$). One can notice that for applications with particle moving through the channel, f_D, varies and $\overrightarrow{F_d}$ can change during particle displacement [23]. This coefficient is frequently ignored for experiments in which the particle radius is relatively small compared to the dimensions of the channel. In case of cell labeled with magnetic particle, the apparent radius can be estimated according to the size of magnetic particles relative to that of the cells.

In most microfluidic applications, the fluid flow profile is not uniform but varies along the channel section (see laminar flow in Chap. 2). However, particles diameter being usually smaller than dimensions of microfluidic channel dimensions, the fluid velocity is considered relatively constant across the particle [23]. The drag force, given by Eq. (7.25), is then estimated at a time t, with particle velocity at t and fluid flow velocity at the position of the particle at t. Most of the publications related to magnetophoretic functions in microfluidic devices assume that the fluid has an average velocity in the entire channel section. See Chap. 2 to take into account v_f profile depending on the position of the particle in that channel for various section shape i.e. rectangular, triangular, cylindrical and aspect ratio.

Drag force is typically in the order of few to few tens of pN in microfluidic devices. For example, $F_d \approx 8.4$ pN for 1 μm diameter particle flowing at 1 mm/s in a fluid with a viscosity of 0.89 mPa·s.

7.3.3 Gravitational and Buoyance Forces

The gravitational force and the associated buoyance forces are expressed as [19]:

$$\overrightarrow{F_g} + \overrightarrow{F_b} = -V_p(\rho_p - \rho_f)\overrightarrow{g}$$

(7.27)

with ρ_p and ρ_f, the density of the particle and the solution, respectively, and $\overrightarrow{g}$ the acceleration due to gravity.

Gravitational force and buoyance forces are neglected for sub-micrometer or nanoscale particles [19, 24]. Indeed, they are much lower than magnetic forces, as illustrated here: 1 μm diameter Fe_3O_4 particle $(\rho_p = 5000$ kg/m$^3)$ flowing in water $(\rho_f = 1000$ kg/m$^3)$, experiences $F_g = 2.56\,10^{-2}$ pN and $F_b = 0.51\,10^{-2}$ pN,

several order of magnitude below applied magnetic forces. For larger particles, typically $R_p > 5\,\mu m$, these forces should be considered.

7.3.4 Other Forces

Other forces (interactions of the particles with their environment: other particles, channel walls, fluid) contribute to the overall trajectory of magnetic particles in a magnetophoretic microfluidic device [25]. Particle/micro-channel wall interactions result from electrostatic and electrodynamic (van der Waals) forces experienced by particles in solution. Indeed, particle and micro-channel walls in contact with electrolytic solution can present a surface charge that induces a double-layer at their surface and their overlapping induces electrostatic interactions [19]. Van der Waals force, on its hand, originates from attractive electromagnetic interaction between electrical dipole and/or induced dipoles [19]. Both forces can generate unwanted particle sticking to the micro-channel walls. This can be avoided by modifying the pH and the ionic strength of the solution or by coating micro-channel wall or particle surfaces with proteins (Bovine Serum Albumin, BSA for example) [1]. These forces quickly decrease as the distance between surfaces increases and are negligible at distances greater than tens of nanometers. Particle/particle interactions can be electrostatic and magnetic. Electrostatics ones, generated by the electric double-layers, are repulsive forces whereas magnetic interactions between particles can lead to the creation of particle clusters that possess their own dynamics [1]. These inter-particle effects as well as particle/fluid interactions are usually ignored for particle suspension at low volume concentration [25, 26]. If these interactions are considered, they give rise to a complex model solved numerically.

7.3.5 Particle Transport Models

All the forementioned forces have an effect on particle transport and two models are used to predict particle trajectories depending on whether Brownian motion is neglected or not. Particles suspended in a fluid undergo random collisions with fluid molecules, generating a random movement of particles, the Brownian motion. Particle diffusion due to Brownian motion is neglected for particles having diameter greater than tens of nanometer. Gerber and co-workers [26] defined a criterion to estimate particle diameter, D_p, below which Brownian motion influences particle displacement:

$$\left|\overrightarrow{F}\right| \cdot D_p \leq k_B \cdot T \tag{7.28}$$

$\left| \overrightarrow{F} \right|$ being the magnitude of the total force acting on the particle. For instance, Gerber et al. estimated a critical particle diameter of 40 nm for the capture of Fe_3O_4 particles in water. For particles with a diameter below or equal to D_p, motion of individual particle is predicted using drift-diffusion analysis, whereas for particle with diameter larger than D_p, Brownian motion is neglected and classical Newtonian physics is employed to foresee particle trajectory.

In the first case, because of thermal agitation and diffusion, particle transport cannot be precisely monitored and a statistic approach must be used to predict their trajectories. Particle transport is modeled using a drift-diffusion equation for the particle volume concentration c:

$$\frac{\partial c}{\partial t} = \overrightarrow{\nabla} \cdot \overrightarrow{J} = 0 \tag{7.29}$$

where $\overrightarrow{J} = \overrightarrow{J}_D + \overrightarrow{J}_F$ is the total flux of particles, which includes a contribution $\overrightarrow{J}_D = -D\overrightarrow{\nabla}c$ due to diffusion, and a contribution $\overrightarrow{J}_F = c\overrightarrow{U}$ due to the drift of particle under the influence of applied forces. D is the diffusion coefficient with $D = \gamma kT$, where γ is the mobility of a particle. $\overrightarrow{U}$ is the drift velocity, with $\overrightarrow{U} = \gamma \overrightarrow{F}$, where $\overrightarrow{F} = \overrightarrow{F_m} + \overrightarrow{F_d} + \overrightarrow{F_g} + \overrightarrow{F_b} + \cdots$, is the total force acting on particle. Equation 7.29 can be written as follow:

$$\frac{\partial c}{\partial t} = D\overrightarrow{\nabla}^2 c - \gamma c \overrightarrow{\nabla} \cdot \overrightarrow{F} \tag{7.30}$$

In most applications, Brownian motion is neglected and this model is rarely used in literature. For details to solve Drift-diffusion transport see initial work of Gerber [27], Fletcher [28], and more recently wok of Furlani [29].

The second model is the most commonly used in literature, as micro- and nano-objects that are mainly manipulated in magnetophoretic microsystems have a diameter larger than D_p. This model uses Newton's second law, to predict particle trajectory, as expressed in Eq. (7.31):

$$m_p \frac{d\overrightarrow{v}_p}{dt} = \sum \text{forces} = \overrightarrow{F}_m + \overrightarrow{F}_d + \overrightarrow{F}_g + \overrightarrow{F}_b + \cdots \tag{7.31}$$

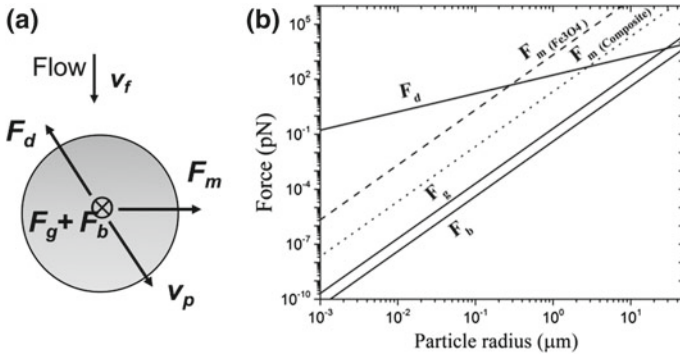where m_p is the mass of the particle.

For sub-micrometer sized particles, the initial term, $m_p \frac{d\overrightarrow{v}_p}{dt}$, is often ignored due to their small mass [30, 31]. Thereby, for the inertial term to be considered particle with a mass of 1 pg should have acceleration above 100 m/s^2, which is unusually large for microfluidic applications. Considering expression of the different forces, Eq. (7.31) can be expressed as follow:

$$m_p \frac{d\overrightarrow{v}_p}{dt} = \mu_0\left(\overrightarrow{m} \cdot \overrightarrow{\nabla}\right)\overrightarrow{H} + 6\pi\eta R_p\left(\overrightarrow{v}_f - \overrightarrow{v}_p\right)f_D - V_p\left(\rho_p - \rho_f\right)\overrightarrow{g} \qquad (7.32)$$

The balance of forces can be tuned by modifying particle properties $\left(R_p, M_s, \rho_p, \chi_p\right)$, fluid properties $\left(\eta, \rho_f, \chi_f\right)$ and the magnetic source (B).

A schematic reporting the main forces experienced by particles in magnetophoretic microsystems is reported in Fig. 7.7a (direction of forces being arbitrary). Figure 7.7b also reports order of magnitude of forces applied on particle according to its size, in typical microfluidic device operating conditions. For magnetophoretic force, we considered that magnetic particles are saturated, and two cases were calculated: the case of Fe_3O_4 particles of which maximum size reach in general few tens of nanometers, and the case of composite particles, composed of a polymer matrix and Fe_3O_4 nanoparticles, of which size can reach tens of micrometers. Based on the choices made, it results that magnetophoretic force is mainly in competition with the drag force. In most publications one considers that the particle magnetization is not saturated, and so the balance of forces can be expressed as follows:

$$\mu_0 V_p \Delta\chi\left(\overrightarrow{H} \cdot \overrightarrow{\nabla}\right)\overrightarrow{H} = 6\pi\eta R_p\left(\overrightarrow{v}_f - \overrightarrow{v}_p\right)f_D \qquad (7.33)$$

Fig. 7.7 **a** Schematic representation of forces experienced by a particle inside magnetophoretic device (arbitrary direction of forces) **b** Order of magnitude of forces as functions of particle radius for following settled particles parameters and fluidic and magnetic conditions: particle density of $\rho_p = 5000$ kg/m^3 (Fe_3O_4) flowing in water ($\rho_f = 1000$ kg/m^3, $\eta = 0.89$ mPa.s), with a velocity of 1 mm/s and submitted to a magnetic field gradient of $\nabla B = 10^3$ T.m^{-1}. For calculus, we considered that two type of magnetic particles that are saturated, Fe_3O_4 particles with magnetization at saturation $M_s = 510$ kA·m^{-1} (F_m, dash), and composite particles (1 vol.% of Fe_3O_4 nanoparticles in a polymer matrix) with $M_s = 5.1$ kA·m^{-1} (F_m, dot)

## 7.4   Implementation of Magnetophoresis in Microsystems

We will focus in this section on the integration of magnetic flux sources in microsystems, which will be used as the remote control.

7.4.1   Sources of Magnetic Field and Magnetic Field Gradient at the Micrometer Scale

To start with, it is worth taking a look at an estimate of the magnitude of the magnetophoretic force. A strong centimeter sized magnet, like the strongest NdFeB-based commercial ones, generates a magnetic field gradient of the order of 10 T/m, and a magnetic field of few 0.1 T close to its surface. Therefore, the force per volume of target object (with magnetization of 100 kA·m^{-1}) will be of the order of 10^{-21} N/nm^3. For particles with a size of 10 nm, this leads to a force in the range of 1 aN (1 attoNewton = 10^{-18} N), a value comparable to the gravity force acting on them. In order to efficiently manipulate nanosized object, it is then of first importance to generate strong magnetic field gradients, and the way to do so is to scale down the magnetic flux source to the micrometer scale.

7.4.1.1   A Variety of Magnetic Field Sources

A magnetic field can be produced by a permanent magnet or an electrical current passing through a coil. These sources of magnetic stray field can be combined with magnetic concentrators that will focus the flux lines due to their large magnetic susceptibility, producing field gradient in their surroundings. Figure 7.8 illustrates the three main approaches that are used to create magnetic field gradients in microsystems.
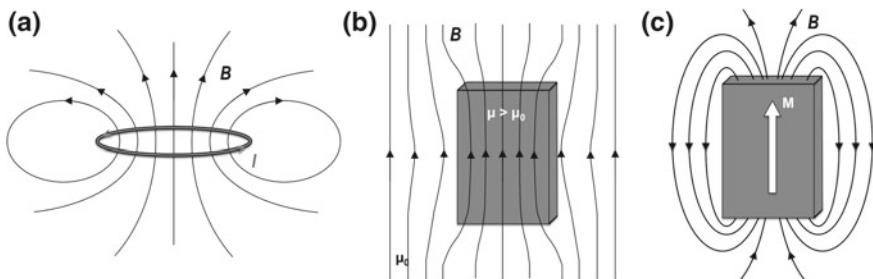
Fig. 7.8   The three reported solutions to generate magnetic field gradients at the micrometer scale: **a** micro-coils made of conducting materials [32], **b** micro-concentrators of magnetic flux made of magnetically-soft materials [33] and permanent micro-magnets made of magnetically-hard materials [34]

7.4.1.2   Downscaling a Magnetic Field Source

Considering a uniformly magnetized object, the field that emanates from it depends on its magnetization and its shape. The magnetization is a bulk property, it does not depend on the size of the object: a large magnet and a small magnet with the same magnetization are capable of creating similar magnetic field around them. On the other hand, the distance on which the magnetic stray field decays scales with the size of the object. Therefore, there is a remarkable advantage to reduce the size of magnetic flux sources as it increases the gradient of the produced magnetic stray field. Figure 7.9 shows the pattern of magnetic stray field around a magnet with a square section of side a, magnetized upwards.

In other words, reducing the size of a magnet by a factor k multiplies the maximum field gradient by k. For micrometer size magnets, the stray field gradient is in the range of 10^3–10^6 T/m. For the same target particle as considered in the introduction of this section, the force that was 1 aN with a centimeter sized magnet, is increased to the range of 1–10^3 fN (1 fN = 10^{-15} N), a value well greater than the gravity force.

Interestingly, downscaling coils is also favorable as the admissible current density can be increased while reducing the size of the conductor. Indeed, Joule heating scales with the volume of the conductor whereas cooling losses through heat flow is proportional to the surface [35].
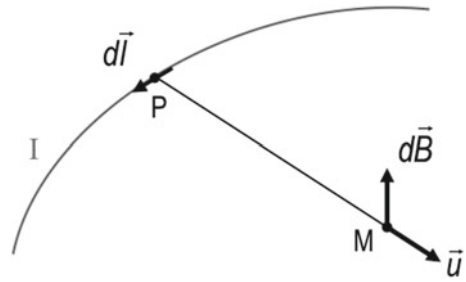
7.4.2   Micro-Coils

Micro-coils are tiny wires of electrical conductor. The building block is a current loop, as illustrated in Fig. 7.10, which can be added up in a planar spiral [36, 37], a 3D solenoid [38], so as to increase the produced flux intensity. Complying with the

Fig. 7.9 Simulated stray field B produced by a magnet with a square section of side a, with a remanent induction of 1.17 T (comparable to the one of NdFeB magnets). The hollow arrow indicates the direction of the magnetization
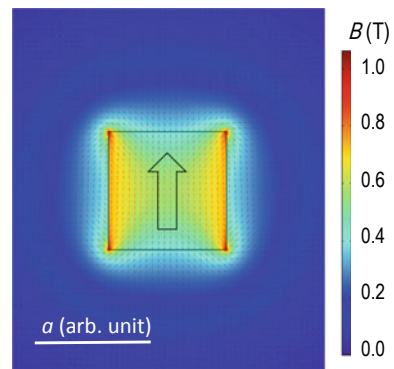
Fig. 7.10 Schematics of the magnetic induction B induced by an electric conductor

framework of this chapter, we will only consider micro-coils as micro-sources of magnetic flux, which differs from their first application as probe heads in magnetic resonance devices [39].

The magnetic induction B created at a point M of the space by an electric circuit element positioned at a point P is given by the Biot-Savart law (7.34):

$$d\vec{B}_M = \frac{\mu_0}{4\pi} \frac{Id\vec{l} \times \vec{u}}{r^2} \tag{7.34}$$

$\vec{u}$ is the unit vector in the plane of the circuit and perpendicular to the element $\vec{dl}$, r the distance from the current element (P) to the considered point (M) and I the current circulating in the element.

It comes that the magnetic induction B generated in the center of a planar coil with N_S windings of radius r is given by:

$$B = \frac{\mu_0 I}{2r} N_S \tag{7.35}$$

The magnitude of the induction increases with the current, the number and the density of windings. However electric current flowing in a resistive wire inevitably produces heat that is called Joule, ohmic or resistive heating. This limits the current intensity but also the number of windings as the resistance of the coil scales with the length of the conductor. The maximum amplitude of magnetic induction reached with micro-coils is in the range of 1 to 10 mT. It could be enhanced by adding a magnetic core at the center that would concentrate the flux, as for bulk electromagnets.

When the micro-coil design integrates several turns, independently to the selected geometry, classical approach combining electrodeposition and photolithography leads to relatively tedious processes, as compared to the fabrication of other magnetic flux micro-sources. It is interesting to note that this could be overcome by exploiting the complex and fine structures in nature, as demonstrated by Kamata et al., who prepared micro-coils using helical microalgae as a biotemplate [40].

Due to relatively low performances in static conditions with respect to the other options, micro-coils are rarely used in this framework but have a great potential for actuators operating at high frequency.

Moreover, the possibility to alternate the produced flux at a time scale below the relaxation times of the superparamagnetic particles could be a way to exploit the bi-directionality of the magnetic force and thus open a new route of development.

7.4.3 Magnetic Flux Micro-sources from Ferromagnets

Ferromagnets are divided into uniformly magnetized regions, called Weiss domains, separated by domain walls. The driving force of domain formation is the minimization of magnetostatic energy, which is the energy stored in the magnetic stray field emanating from the ferromagnet. Schematics in Fig. 7.11 illustrate how closure domain structure (Fig. 7.11b) cancels out the magnetic stray field. The closure domain structure is reached by cooling the ferromagnet across its Curie temperature. The focus of this section is the use of ferromagnets as magnetic field and magnetic field gradient sources and therefore we will consider them in the magnetized configuration (Fig. 7.11a). As previously discussed in Sect. 7.2.1, we will distinguish two types of ferromagnets, the so-called hard magnetic materials that can remain magnetized in the absence of applied field and the so-called soft magnetic materials of which the domain structure systematically falls in a configuration like in Fig. 7.11b at zero field. The former type can be used to prepare permanent micromagnets while the latter serves for micro-concentrators of magnetic flux.

Fig. 7.11 Magnetic domain structure in ferromagnets and magnetic stray field (red lines) in two limit cases: **a** a single domain and **b** a closure domain structure
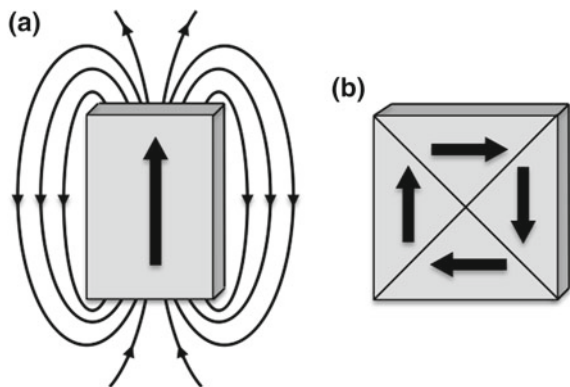
7.4.3.1 Micromagnets

Permanent magnets define objects that produce magnetic stray field in their environment, in the absence of external excitation, such as a circulating current or a magnetic field. This particularity implies that the predominant constituting phase retains a fraction of its magnetization, which is called the remanent magnetization. An important ingredient is the magnetic anisotropy. The large majority of produced permanent magnets nowadays get their hard properties from a large magneto-crystalline anisotropy. When looking back at the evolution of permanent magnet performances over the last century, the main achievements came with the discovery of new hard magnetic compounds. The main breakthrough came in the 1950's with the discovery of ferrimagnetic hexagonal ferrites, of which the high anisotropy permits to manufacture them in any shape and so opening new possibilities for device designs.

The magnetic performances of magnets are generally assessed by a figure of merit called the energy product, denoted $(BH)_{max}$, which scales the amount of energy stored in the stray field. It corresponds to a working point on the induction curve B(H) that maximizes the area under the curve in its second quadrant (see Fig. 7.12). A high $(BH)_{max}$ reflects a high enough resistance to demagnetization and a large magnetization. Beyond a certain value of coercive field H_C, the maximum energy product is only a function of M. In fact a hard magnetic phase is characterized by a maximum theoretical energy product that is:

$$(BH)_{MAX} = \frac{1}{4}\mu_0 M_S^2 \tag{7.36}$$

Table 7.6 gives characteristic parameters for some hard magnetic substances. When using magnets as magnetic flux sources, one exploits its stray field, which is

Fig. 7.12 Characteristic magnetization and magnetic induction curves of a permanent magnet
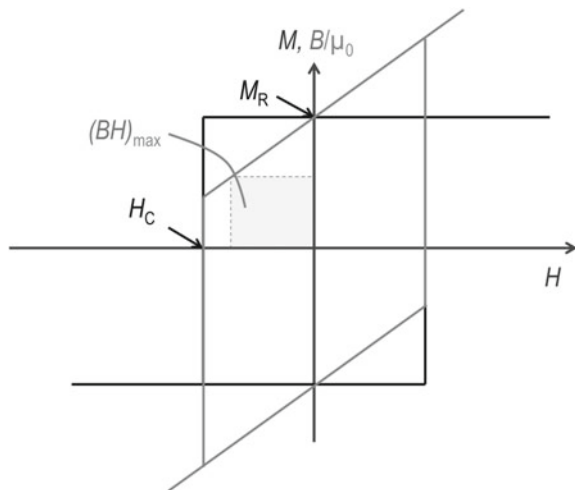
Table 7.6 Characteristic parameters of some hard magnetic phases [41, 42]

Material	M_S (kA/m)	Theoretical $(BH)_{MAX}$ (kJ·m^{-3})
$SrFe_{12}O_{19}$–$BaFe_{12}O_{19}$	200–380	12–45
Alnico 5	1110	(in practice: ≤ 50)
hcp–Co	1370	–
Fe_3C	1190	–
$L1_0$–CoPt	810	200
$L1_0$–FePt	1140	406
$SmCo_5$	860	231
$Nd_2Fe_{14}B$	1280	512
$B8_1$–MnBi	580	106
$L1_0$–MnAl	600	113

the field created outside its volume. In general, the stray field is calculated using either the Amperian approach, in which the magnetization is replaced by an equivalent distribution of current density, or the Coulombian approach, in which the magnetization is replaced by an equivalent distribution of magnetic charges. The two approaches are illustrated in Fig. 7.13 for a uniformly magnetized cubic magnet.

The calculation of magnetic stray field is general performed by finite element method, though analytical solutions for simple shapes can be found in literature [43].

Fabrication of Bulk Magnets

Bulk magnets are generally prepared by powder metallurgical processes, which can be briefly summarized as follows: (1) a mixture of the raw elements is first molten in furnaces and cooled down to form cast magnets, (2) the obtained material is then either ball milled or jet milled to obtain fine powders, with particle sizes ranging from few micrometers up to hundreds of micrometers, (3) this powder is then pressed into molds and heated to be sintered. The as obtained «sintered magnets»

Fig. 7.13 Equivalent approaches for the calculation of the magnetic stray field emanating from a uniformly magnetized magnet with a square section **a** fields produced by an equivalent distribution of currents **b** and an equivalent distribution of charges **c**

Sintered magnets

(a) Isotropic   (b) Oriented

Bonded magnets

(c) Isotropic   (d) Oriented
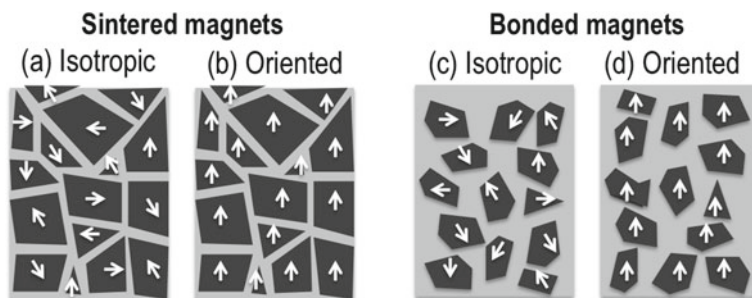
Fig. 7.14 Schematics of the microstructure of bulk-manufactured magnet

are relatively dense (density greater than 90%) but brittle. A solution to obtain more mechanically robust magnets is to bond the fine powder with a polymer, thus facilitating magnets shaping, for example by injection moulding, which opens up new possibilities for device designers. In addition, these so called «bonded magnets» show higher resistance to corrosion. However, they present less magnetization than their sintered magnets counterparts because of the relatively large volume fraction of non-magnetic binder (the volume fraction of the magnetic powder is typically 60–80%). Typical binders used are epoxy resin, polyamides or nitrile rubbers. Schematics of Fig. 7.14 show the different microstructures of magnets.

Classification of Permanent Magnets

One can put magnets in four categories, according to the constituting elements and structure: hexagonal ferrites, alnicos, metal alloys and rare-earth intermetallics. They all have their advantages and weaknesses. Hard hexagonal ferrites have the general formula $MO–6(Fe_2O_3)$, with M being mostly Sr or Ba. They are produced nowadays in large quantity, in the range of 10^6 tons/year. They have limited performances but present the great advantages of being cheap and excellent resistance to corrosion. Alnicos are nanostructured materials consisting of Fe–Co needles in a non magnetic Al-Ni matrix, with traces of Cu and Ti. They are obtained by spinodal decomposition and the anisotropic nanostructure is obtained by means of thermal process under magnetic field. They present good thermal stability, relatively high magnetization but suffer from relatively low resistance to demagnetization and therefore are generally found in rod shapes. Hard metal alloys are usually made by direct casting of $3d$ transition metal elements taken among Mn, Fe, Co, Ni with other metallic elements, of various types like Ga, Al, Pd, Pt, Bi. They have in common a non-cubic structure. Binary $L1_0$ alloys like FePt and CoPt present impressive hard magnetic properties and good resistance to corrosion but suffer from the high cost of Pt. Rare-earth intermetallic magnets, like NdFeB–based magnet, show the highest magnetic performances and are relatively low cost. Their main weakness is their poor resistance to corrosion, which requires coating them in order to limit degradation over time. For use in microfluidic systems intended for biology, the operating temperature window is rather restricted to a narrow range,

typically 10–40 °C, where all magnets described above can be used with relatively steady performances.

Integration of Permanent Micromagnets in Microsystems

The integration of permanent magnets in microsystems is challenging mainly because hard magnetic properties are highly sensitive to both chemical composition (alloy composition, structure, chemical order) and microstructure (grain size, grain boundary phases, defects). This usually implies some preparation constraints like thermal treatments, or sometimes processing steps under magnetic field. In addition, once prepared it is necessary to apply a strong external magnetic field so that to get a maximum remanent magnetization.

Micro-Magnets Fabrication Routes

Machining bulk high performance sintered magnets to obtain sub-millimeter sized magnets, for example by spark cut, is restricted to relatively coarse features as inevitable degradation of the surface will be detrimental for the magnetic hardness. In addition, machining or deforming bulk magnets is not suitable for preparing micro-pattern arrays.

Instead, two main approaches were developed to fabricate such micro-magnet arrays: patterning of films or powder positioning.

Several film deposition and patterning methods can be used, including sputtering [44], pulsed-laser deposition [45], evaporation [46], or electrochemical deposition [47]. Electro-deposition has been found as an efficient way to prepare thick films of rare earth-free magnetic films. Pulsed laser deposition technique is usually restricted to relatively low deposition rate and relatively small deposition areas, and is difficult to scale up. Sputtering, like electrochemical deposition, can be adapted for deposition on large areas and with relatively high deposition rates of 10–40 µm/h [48].

Films can be topographically patterned depositing them on thick resist masks and then performing lift-off [49], or else onto pre-etched substrates (predominantly silicon) using deep reactive ion etching [50]. For hard magnetic compounds that are less sensitive to corrosion (rare-earth free magnetic films), an additional option is to pattern the films, post deposition, through wet etching or focused ion beam. The as-obtained arrays of permanent micro-magnets are heated to form the hard magnetic phase, either during deposition, or with post-deposition annealing, and then magnetized in the unidirectional field of a superconducting coil to reach the full remanence of the micro-magnets.

Local change of the structure or of the chemical order can be another route to obtain patterned hard magnetic films at the micrometer scale. As an example, Okuda et al. induced local magnetic hardness in NdFeB film that were initially poorly crystallized and so magnetically soft, by employing pulsed annealing through a mask [51].

Other approaches were developed to create such multipolar structures in continuous magnet films, magnetized locally in opposite directions. To reverse the magnetization in specific zones, one can use electrical pulses in conducting wires positioned in contact to the film [52, 53], or else using the so-called

thermo-magnetic patterning [54], which consists in locally reversing the magnetization of a uniformly magnetized film by heating micrometer-sized areas with a laser pulse through a mask, under moderate magnetic field. The process is schematized in Fig. 7.15. The advantages of this method are that it creates multipolar configuration that is favorable for magnetic stray field strength and the absence of topography patterns facilitates the integration in devices. The main disadvantage is the rather limited reported depth (less than 2 μm) of the magnetization reversal. Other means to reverse locally the magnetization of hard films have been proposed since, using soft ferromagnetic masks that locally concentrates magnetic flux in the opposite direction with respect to the initial film magnetization direction [55].

Film-based techniques offer the great advantages of reproducibility, and fine controls over geometries and microstructuration. However, they suffer from a tendency of peeling off from the substrate due to mechanical stress building-up in thick deposited films. Also, their fabrication processes are relatively expensive, slow and tedious. As the hard magnetic phases are usually obtained after heat treatment, the thermal expansion coefficients of the film and the substrate may set an upper limit on the film thickness.

Methods to transfer well-defined arrays of film-based structures in polymer matrix were developed in order to ease the integration in polymer-based microsystems [56–59].

In contrast to film-based methods, powder-based methods employ particles used in bulk-manufactured magnet industry as building blocks, which have already desired hard magnetic properties. Bonded micro-magnet arrays are generally obtained by filling cavities present in resist masks or pre-etched silicon substrates with a mixture of magnetic powder and a polymer binder. Among the most ubiquitous techniques of fabrication, one can cite replica molding, squeegee coating or screen printing. Other techniques like inkjet printing do not use physical master. Note that generally the powder-based approaches integrate a process step with an applied magnetic field in order to align the particles and confer an overall anisotropy to the bonded micro-patterns. In order to go down in sizes, it is also possible
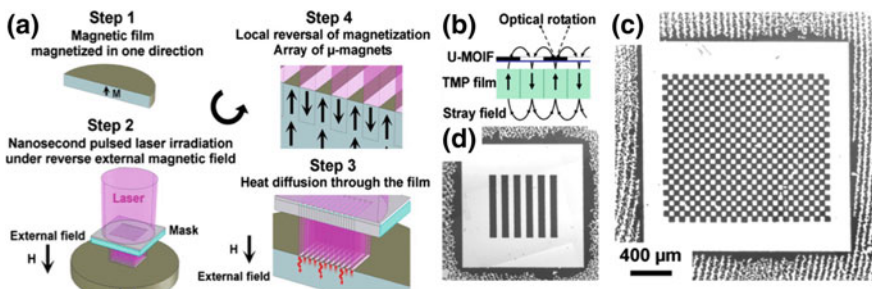
Fig. 7.15 Thermo-Magnetic Patterning process developed by Dumas-Bouchiat et al. Reprinted from [54], with the permission of AIP Publishing

to use magnetic molds to precisely position magnetic particles on a surface and then transfer the formed pattern arrays in a medium like a polymer [60].

Many efforts were done to develop high performance micro-magnets, in various contexts and geometries. The performances are assessed by local characterization of the stray field, and its gradient using magneto-optical indicator films (MOIF) [59], Hall micro-probes [56, 61] or measurements of forces exerted on "colloidal tips" in a magnetic force microscopy set up.

In the context of microfluidic systems integrating magnetophoretic forces, the micro-magnets offer the great advantage of producing strong stray fields without any external excitation, which is beneficial for compact and low-power consumption devices. The main disadvantage of micro-magnets is that the generated force pattern cannot be easily modulated in real-time. This can be an issue to consider when releasing the trapped object is desired. Using magnetically-soft ferromagnets can be a way to overcome this limitation.

7.4.3.2 Micro-Concentrators of Magnetic Flux

The "micro-magnet" term is often abusively used to refer magnetically-soft micro-patterns, although a magnet is characterized by its ability to retain a fraction of its magnetization when the field is removed. Here we make the distinction between micro-magnets and magnetically-soft micro-patterns that only become magnetized in the presence of an external magnetic field. They are used to concentrate an external magnetic flux that can be delivered either by an electric circuit or a permanent magnet. In the absence of external field, the soft magnetic object structure collapses in multi-domains and there is no stray field. Micro-concentrators are characterized by a large change of their magnetization state when submitted to a relatively low external magnetic field. The performance of the flux guide is related to the intrinsic magnetic permeability μ of the constituting material. The higher the magnetic permeability, the more concentrated the magnetic flux is. In addition to the permeability, an important parameter is the maximum flux the material can concentrate, which is determined by the spontaneous magnetization M_S. Figure 7.16 shows the magnetic flux inside and nearby a soft magnetic material that is magnetized in a field of 0.2 T created by bulk magnets.

Table 7.7 presents some values of magnetization M_S and magnetic relative permeability μ_r of some commonly encountered magnetically-soft materials at room temperature. One can find several classes of magnetically-soft materials: low-carbon mild steels, Fe-Ni alloys, Co-Fe alloys, soft ferrites. They generally result from a compromise between high saturation magnetization and the addition of non-magnetic elements to increase their magnetic softness (among which Al, Si, C, Mo, Cu). Unlike hard magnetic compounds, additional elements are intended to render the alloy amorphous or reduce chemical ordering. These elements can also help to increase electrical resistance so that to improve high frequency performances. In the bulk state, grain-orientation, lamination, annealing under magnetic

Fig. 7.16 Simulated stray
field *B* produced by a cubic
magnetic flux guide of side *a*,
in the gap between two
permanent magnets
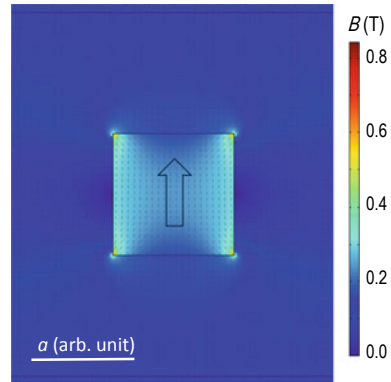
Table 7.7 Characteristic parameters of some magnetically-soft materials [13, 62, 63]

Material	M_S (kA/m)	μ_r
Soft Fe	1710	300–5,000
Hypernik (Ni$_{50}$Fe$_{50}$)	1270	6,000–40,000
Metglas 2826 (Ni$_{50}$Fe$_{50}$-based)	700	50,000–800,000
Metglas 2714 (Co-based)	450	80,000–1,000,000
Permalloy (Ni$_{80}$Fe$_{20}$)	830	8,000–100,000
Supermalloy (Ni$_{80}$Fe$_{15}$Mo$_5$)	700	100,000–300,000
Mumetal (Ni$_{77}$Fe$_{16}$Cu$_5$Mo$_2$)	520	20,000–100,000
Ni	480	100–600
Mn-Zn ferrites	290–400	500–10,000
Ni-Zn ferrites	200–330	10–1,000

field can be used to induce anisotropy and thus improve magnetic permeability in a
desired direction.

Dependence of the Magnetic Response on the Patterns Shape

When one wants to integrate micro-sources of magnetic field gradient in
microsystems, it is of first importance to consider the shape contribution to the
apparent susceptibility (M/H_{ext}), which will predominate in most cases.

In general the demagnetizing field H_d is not uniform within the volume of the
object and the use of finite element modeling to describe the magnetic response to
an external field is necessary. The demagnetizing field is uniform within ellipsoid
shapes (of axes 2*a*, 2*b* and 2*c*, see Fig. 7.17) and it is thus possible to get a rapid
estimate of the demagnetizing field by considering the closest ellipsoid shape to the
given object. Table 7.8 gives the analytical expressions of the demagnetizing fac-
tors for revolution ellipsoids. The apparent susceptibility is then simply related to
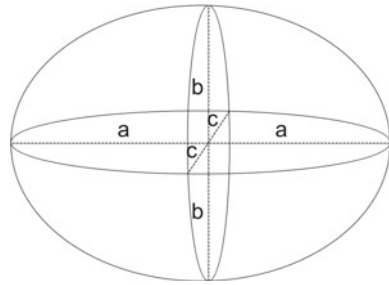
Fig. 7.17 General ellipsoid

**Table 7.8** Demagnetizing factors for revolution ellipsoids [64]

Ellipsoid shape	Demagnetizing factors
Prolate (cigar shape), with $s = c/a$ $a = b < c$	$N_c = \frac{1}{s^2-1}\left[\frac{s}{\sqrt{s^2-1}}ln\left(s+\sqrt{s^2-1}\right)-1\right]$ $N_a = N_b = \frac{1-N_c}{2}$
Sphere $a = b = c$	$N_a = N_b = N_c = \frac{1}{3}$
Oblate $a < b = c$	$N_c = N_b = \frac{1}{2(s^2-1)}\left[\frac{s^2}{\sqrt{s^2-1}}arcsin\left(\frac{\sqrt{s^2-1}}{s}\right)-1\right]$ $N_a = 1 - 2N_c$

the intrinsic value and the demagnetizing factors along the three orthogonal axes satisfy:

$$N_a + N_b + N_c = 1 \qquad (7.37)$$

Fabrication of soft micro-patterns In magnetophoretic microsystems, magnetic flux micro-concentrators are certainly the most used, and this can be partly explained by their ease of micro-fabrication compared to hard magnetic phases that require thermal treatment. Poor cristallinity and low degree of chemical ordering, which is generally obtained in the as prepared state, is not detrimental, and even can be favorable for magnetic softness. This is especially true when we restrict the use to static conditions (variation of the applied field in the Hz range), which is the general case for microfluidic systems integrating magnetophoretic functions.

Figure 7.18 shows some experimental realizations. Apart from multipolar micro-patterning, all the aforementioned micro-fabrication techniques described in the section devoted to micro-magnet arrays can be applied to micro-concentrators. Film-based methods, where films were micro-patterned to prepare batches of well-defined and fully dense micro-concentrators, are largely employed. Films are prepared by electro-deposition, sputtering, evaporation or pulsed laser deposition [65]. As for micro-magnets, thicknesses ranging from 1 to 100 μm are desired and thus high rate deposition techniques are suitable. Micro-patterning can then be achieved by different methods, including lift-off using photoresist masks [66] or by depositing the films on pre-etched substrates [56].
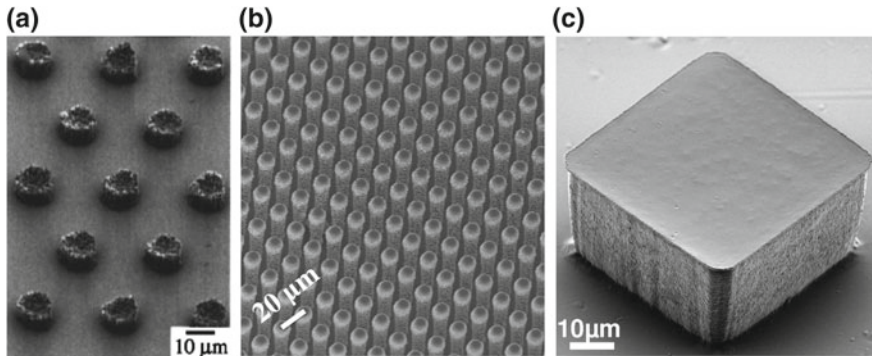
Fig. 7.18 Micro-concentrators prepared by film micro-patterning: Ni structures made by lift-off (reprinted from [66], with the permission of AIP Publishing) **a** FeCo structures made by deposition on pre-etched Si substrates [56] **b** and iPDMS pillar made by soft lithography **c** (reprinted from [67], with the permission of AIP Publishing)

However, film-based methods suffer from high processing cost, and also are limited to suitable substrates using sometimes a buffer layer to ensure adhesion.

In contrast, powder compaction and positioning offer the great advantage of low cost processes. Like for permanent micro-magnets, soft powder-loaded polymer composites can be micro-patterned using the same methods as described for composites with hard magnetic powder, including replica molding [67], or ink printing [68, 69]. However, low compaction inevitably leads to additional demagnetizing field effects at the grain scale, which can be detrimental for magnetic susceptibility and so magnetic flux guiding performances. High aspect ratio structures can be obtained by organizing the soft particles in chains within the polymer matrix [70].

Micro-concentrators of magnetic flux constitute an appealing solution as the reachable magnetic forces are comparable to the ones obtained with permanent micro-magnets but they offer in addition the possibility to modulate the force intensity in real time by varying the external flux. Their fabrication and their integration in microsystems are relatively easier than for micro-magnets as the exploited magnetic properties are less sensitive to micro-fabrication processes.

7.5 Magnetophoretic Functions Dedicated to Bio-Analysis

Implementation of magnetophoretic functions in microsystems permit to address numerous biological, medical, chemical and environmental applications. They are part of the enthusiasm of recent years for micro total analysis systems, µTAS. Employed either to control micro-object motion in channels, or involved in the sensing process, magnetic bio-device field of research is very active, and many

researches were published those past years. Objects handled in magnetophoretic devices are magnetic micro- and nano-particles (MMPs and MNPs), magnetically labeled cells and cells presenting intrinsic magnetic properties. Currently, magnetophoretic implementation for biomedical applications is realized following three main strategies, using: (i) external permanent magnet, (ii) integrated permanent magnets and (iii) integrated micro-concentrators of magnetic flux. As explained in Sect. 7.3.1, miniaturization of magnetic material down to micron-scale permits to obtain high magnetic field gradient separator (HGMS) which can be required when small particles or particles with low magnetization are employed in microfluidic systems.

In this section, we will describe these three different approaches by highlighting the type of manipulated micro-object. The first paragraph is focused on magnetic particles and the second paragraph deals with magnetic bio-devices.

7.5.1 Magnetic Micro- and Nano-Particles Used in Microsystems

Magnetic particles (MPs) research fields are multidisciplinary. They require inputs from chemistry, biology, physics, medicine, engineering, whether it concerns their magnetic properties, synthesis, surface functionalization, magnetophoretic manipulation or applications. MNPs possess high surface-to-volume ratio, that is advantageous for detection process, and also magnetic properties that allow their manipulation in the sample as their transport for subsequent sensing functions. They are largely used in biomedical applications such as drug targeting, contrast agent for MRI, specific cell labelling and separation, diagnostic and hyperthermia as reported by those reviews [71–75]. They are also largely exploited in environmental applications mainly to perform pollutant removal or detection [76–79]. In microfluidic devices, manipulation of MPs addresses biomedical applications [4, 80], mainly for cell isolation, immunoassay and DNA extraction, but also environmental [81, 82] applications, for toxin or environmental reagent detection or chemical catalysis [83].

Particles must meet some general requirements to be compatible with biomedical analysis, i.e. biocompatibility, biodegradability (for in vivo applications), stability in various medium, narrow size distribution and regular shape that largely impact measurement reproducibility. They may also be superparamagnetic, in order to exhibit large magnetization in presence of applied magnetic field to achieve large magnetophoretic forces; and no coercivity, i.e. no remanent magnetization in absence of magnetic field, to allow a switch off of the magnetophoretic force and a better dispersibility in solution.

Magnetic particles, also called magnetic beads, of different sizes are employed in micro-fluidic devices: nano-particles (10–100 nm), sub-micrometer particles (0.1–1 μm) and micrometer particles (1–50 μm). Iron oxide particles, magnetite and

maghemite particles, are the most commonly used. We can also find particles made of pure ferromagnetic metals, Fe, Ni, or Co, alloys such as Permalloy, $CoPt_3$ or FePt and oxide ferrite such as $M–Fe_2O_4$ (M being, Mg, Zn, Mn, Ni, Co,…). Different particles properties (magnetization at saturation, maximum diameter for nanoparticles to be superparamagnetic, and critical diameter for particle to switch from single to multi-domains) are given in Table 7.9 for various materials [84–86].

MNP preparation involves several steps including particle synthesis, coating or encapsulation and functionalization. MNP synthesis is a very active field of research in literature, and many reviews were published those past years [87–89]. Different synthesis pathways are reported: (i) chemical methods such as co-precipitation and thermal decomposition which are the most commonly used; (ii) physical methods, such as gas-phase deposition and electron beam lithography, which struggle to control particle size down to the nanometer scale; and (iii) more recently, microbial method that exploits the ability of bacteria such as *Thermoanaebacter* species and *Shewanella* species to synthetize Fe_3O_4 NP under anaerobic conditions by the reduction of Fe(III). Currently, co-precipitation is preferred for its simplicity and important yield. If MNP shape uniformity is required as well as a narrow particle size distribution, thermal decomposition is favored. Both methods permit to obtain magnetic nanoparticles with typical size ranging from 2 to 50 nm.

Once particles are synthetized, a protection layer, impenetrable, can prevent MNP from oxidation or erosion and can also reduce metal degradation and related toxicity (Co, Ni, Mn). This results in MNPs with a core-shell structure, a magnetic core, coated by a shell, isolating the core from the environment. Such MNP surface coating may also improve the colloidal and physical stability of the particles. Coating strategies can be basically divided into two approaches: coating with organic shell (polymers and surfactants) and coating with inorganic materials such as carbon, precious metals (e.g. gold) or oxides (e.g. SiO_2). Another approach, which differs from core-shell structure, consists in embedding dispersed MNPs in a dense polymer (e.g. polystyrene) or silica matrix to form composite. Such composite

Table 7.9 Saturation magnetization is given at T = 0 K, the first order anisotropy constant at room temperature. d_{sp} is the calculated maximum diameter for spherical superparamagnetic nanoparticle, D_{crit} is the critical diameter at room temperature which particle switch to multi-domain particle. Adopted from [86–89]

Material	M_S (kA·m^{-1})	K (kJ·m^{-3})	d_{sp} (nm)	D_{crit} (nm)
Fe	1710	48	17	14
Co	1440	410	8	70
Ni	488	−5	32	55
Fe_3O_4	480	−11.13	26	128
γ-Fe_2O_3	400	4.6	–	166
$CoFe_2O_4$	475	180	10	–
$MnFe_2O_4$	560	−2.8	41	–
$NiFe_2O_4$	300	−5.1	33	–

particles can have different structure depending on synthesis process: (i) MNPS can be dispersed in a continuous matrix, (ii) they can be dispersed on the coating of larger particles, like a shell of MNPs, (iii) they can form agglomerates of individual particles that are connected through their protective shells [90]. This approach permits to obtain micron-size particles, typically 0.1–50 μm, that contain more magnetic materials than primary magnetic nano-particle, and permit to reach higher magnetic forces. They are thus largely used in microfluidic systems. One can notice that larger magnetophoretic forces are exerted on larger particles that contain more magnetic material, giving rise on more efficient magnetic functions, but in that case, gravitational forces are also increased and thus may be considered in forces balance.

Finally, particles can be functionalized with specific molecules such as nucleic acids, peptides or proteins to provide bio-functionality in order to perform cell isolation, immunoassay and DNA extraction. Proteins can bind/adsorb to hydrophobic surfaces such as the one of polymer-coated particles. Strong binding between the particle surface and the proteins can also be obtained via specific group at the surface beads such as hydroxyl (–OH), carboxyl (–COOH) and amines (–NH_2) which via an activating agent bind to –NH_2 or –SH groups on the proteins. Bio-functionalization can also be processed via specific and strong complementary recognition interaction such as antigen-antibody or streptavidin-biotin. Various types of functionalized magnetic particles are commercially available [5]. Lists of cancer biomarkers, ligands for viruses and for proteins of biopharmaceutical interest can be found in these articles [5, 84].

As a conclusion, ideal properties of MNPs for bio-devices are:

- superparamagnetic behavior,
- spherical shape and narrow size distribution,
- physico-chemical robustness,
- high binding capacities,
- low non-specific binding,
- minimal cell perturbations, in case of cell labeling, as describe hereafter.

7.5.2 Magnetic Bio-Devices

Magnetic bio-devices are employed for two main types of applications: the detection of bio-molecular markers using magnetic beads, and the manipulation of cells. For both cases, similar methods are employed to implement actives functions (using permanent magnets or micro-concentrators of magnetic flux). The strategies developed to manipulate magnetic target objects are either trapping or deviation towards a dedicated area in the device or towards specific outlet. We will describe now different magnetic bio-devices, which are in a first part dedicated to bio-molecular marker detection, and in a second part, dedicated to cell manipulation.

7.5.2.1 Magnetic Bio-Devices for Bio-Molecular Marker Detection Using Magnetic Micro- or Nano-Particles

Manipulation of MNPs or MMPs in bio-devices are mainly dedicated to the detection of biomarkers such as nucleic acids and proteins. Their detection in blood or serum permit avoiding invasive methods, i.e. biopsy, and their detection at low concentrations allows early diagnosis.

In the case of nucleic acid detection, the sample preparation requires two primary steps, cell separation and lysis, followed by nucleic acid extraction and purification. Cell sorting can be performed using magnetophoresis approach as discussed hereafter. Once cells have been lysed, a purification step can be realized with different microfluidic functions based on filtration, electrostatic interaction, silica-based surface affinity and functionalized magnetic microparticles [91–93]. Steps following DNA extraction such as mixing of reagents, washing particles containing DNA, incubating them in an elution buffer to detach DNA, and proceeding to PCR (polymerase chain reaction) for subsequent quantification can also be performed in microfluidic device [92, 94, 95, 99]. Bio-devices integrating several steps for DNA quantification using digital microfluidic [97, 98] or in-channel approaches [92–94, 96] are reported in literature. Digital microfluidic (DMF) principle is to control fluid as discrete and individual droplets using an array of independent electrodes on a microchip. DNA extraction using DMF present the advantage of high flexibility allowing MNP separation, mixing with reagent, and washing, while limiting reagent consumption [100]. For example, Hung et al. [98] presented a microchip for genomic DNA extraction from whole blood using DMF. The magnetic bead collection and washing procedures are shown in Fig. 7.19A. After beads and the remnant supernatant merged with Wash Buffer 1, an external permanent magnet created a magnetophoretic force on magnetic beads that were collected toward the magnet. By applying a voltage on the opposite side of the droplet, it was split into two droplets, magnetic beads being collected in one droplet. The washing procedure was pursued with another buffer from another droplet. Based on in-channel approach, Strohmeier et al. [93], proposed an innovative method for magnetic beads transport in multiple microfluidic chambers containing reagents necessary for DNA purification. The strategy was based on the coupling of a centrifugal microfluidic LabDisk with a stationary permanent magnet. As shown in Fig. 7.19B, the microfluidic structure is composed of microfluidic chambers, isoradially arranged on a central microfluidic LabDisk. Chambers were first loaded with liquids. Transportation of magnetic beads in successive chambers was achieved by incremental rotation of the LabDisk with respect to the non-rotative permanent magnet. Based on this preliminary work, they developed a fully automated centrifugal-microfluidic LabDisk system, with pre-stored reagents, that performs DNA extraction and PCR for the detection of a panel of bacterial pathogens [99]. The Lab-disk design and the associated Lab-Disk player for point-of care processing are presented in Fig. 7.19C.

DNA extraction can also be achieved using micro-concentrators of magnetic flux. For example, Lou et al. [101] proposed a device for micro-magnetic selection
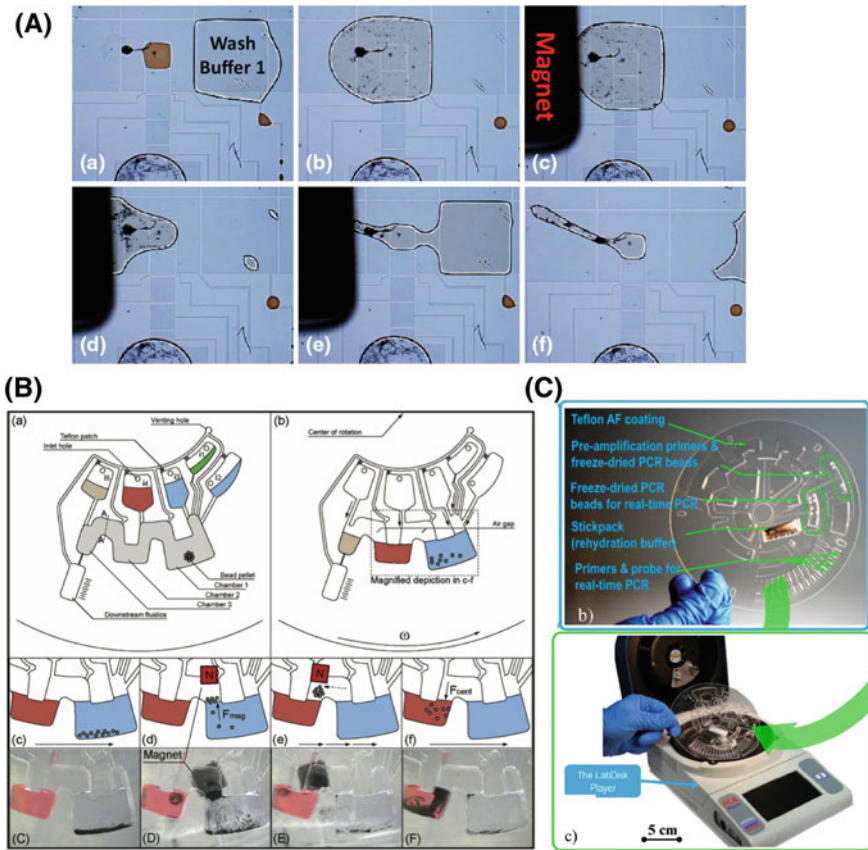
Fig. 7.19 A Magnetic beads collection and washing procedure using DMF (Reproduced from [98], copyright (2015), with permission of Springer); **B** Schematic representation of a centrifugal LabDisk microfluidic structure, and of different steps with associated pictures of the device: **c** beads are centrifuged in chamber 1, **d** LabDisk stopped in a defined position relative to the magnet, beads are attracted by the magnet and move across the air gap between chamber 1 and 2, **e** the Labdisk is rotated of 0.5° while the stationary magnet holds the beads, **f** the LabDisk is accelerated and beads are centrifuged into chamber 2 (Reproduced from [93], with permission of The Royal Society of Chemistry.); **C** Top, LabDisk photo, down, photo of the portable LabDisk-Player for processing the LabDisk at the point-of-care (Reproduced from [99], with permission of The Royal Society of Chemistry)

of aptamers, nucleic acid molecules, in microfluidic channels using micro-fabricated nickel strips. As shown in Fig. 7.20, the device comprises 3 inlets: two were used to introduce in the channel the sample made of magnetic beads bound to the target aptamers and unbound oligonucleotides, and the central inlet was used to introduce a buffer solution. Because of laminar flow, sample and buffer streams did not mix. By positioning an external magnet under the device, Ni strips focused magnetic field lines and created around them regions of high magnetic field

gradient. Forces generated on magnetic beads deviated them from their trajectory towards the center of the channel, whereas, unbound aptamers were directed into the waste outlet. As a consequence, beads with bonded target nucleotides were exited solely by the product outlet.

In the case of proteins, numerous magnetic bio-devices were developed. Different proteins are presents in blood, with concentrations ranging from $pg \cdot mL^{-1}$ to $mg \cdot mL^{-1}$. Low blood sample volume used in microfluidic systems requires techniques with high sensitivity, as no method exists for direct amplification of proteins, as PCR for DNA. Achieving low limit of detection (LOD), is also interesting for detection of toxin and environmental agent in serum, water or food samples. Tekin and Gijs [102] published a review on ultra-sensitive protein detection in microfluidic systems. Immunoassays are mainly used to detect a target protein via the specific recognition between a target antigen (Ag) and an antibody (Ab). Different immunoassay technics are employed, the most commonly used being the sandwich immunoassay.

Magnetic-immunoassay is currently performed as follow in micro-device: Ab-coated magnetic beads are transported, via magnetic field, towards the region in the micro-channel where Ag are localized. After Ab-Ag immunocomplex formation, magnetic beads can be conveyed to the area of detection, which is also a crucial step to reach low LOD. The last step is the Ag detection, which can be performed either without involving magnetic beads [102] i.e. by fluorescence, electrochemistry, (electro)chemiluminescence or mass spectrometry, or by using magnetic beads as labels [102], i.e. by isomagnetophoresis [103], or by monitoring the coverage of a surface by magnetic beads. Microchips using external magnet are
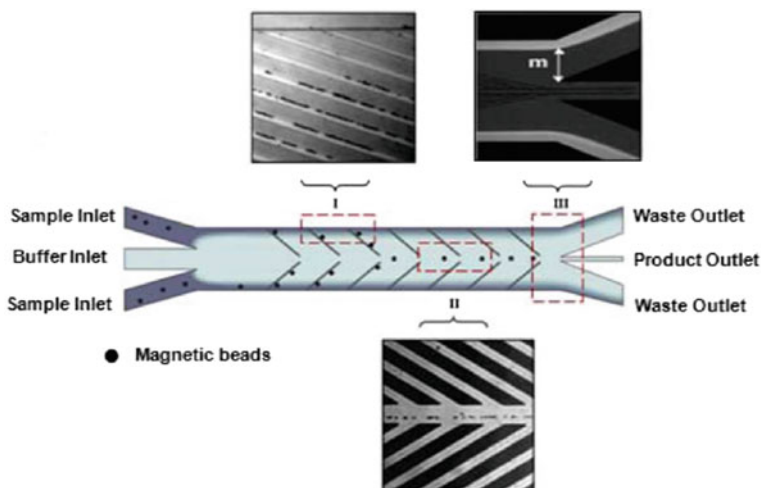
Fig. 7.20 Schematic of the flow pattern and of magnetic beads deflection within the micro-channel. Optical micrographs along the channel demonstrate the separation process (Reproduced from [101], with permission of PNAS)

reported in literature. Indeed, Tekin et al. [104] proposed a system using a magnetic bead surface coverage assay (Fig. 7.21A). First large magnetic beads functionalized with primary Ab specifically captured antigen present in a sample using active microfluidic mixing. In a second step, these beads were exposed to a surface patterned with fixed smaller magnetic beads coated with secondary Ab. A permanent magnet was positioned underneath the device. The generated magnetic field gradient forced larger magnetic beads towards the patterned substrate and biomolecular recognition permitted to trap larger beads on smaller ones. Note that the attractive magnetic interaction between the two types of beads improved Ag-Ab immunocomplex formation. Non-specific adsorption of large magnetic beads was limited by exploiting viscous drag force in the channel after magnet removal. Quantification of antigen concentration was performed by counting the number of bounded large beads. Their immunoassay protocol allowed the detection of (TNF-α) with a LOD of 1 fg·mL^{-1}.

Transport of magnetic beads in micro-channel using external magnet was also reported by Sasso et al. [105]. They developed a system in which magnetic beads were pulled from a reagent stream to the next one in the presence of an external magnet. After this transfer, the solution that carries beads was removed via a waste outlet, and beads flowed into the incubation spiral where Ag-Ab recognition occurred. Phurimsak et al. [106] developed a continuous flow reactor that consists in a microfluidic chamber with co-flowing reagent streams dedicated to C-creatine protein (CRP) detection via a sandwich immunoassay and fluorescent label. Functionalized magnetic particles were deflected across the reaction chamber under the influence of magnetic field gradient due to the presence of an external magnet. They crossed alternating streams of reagents and washing buffers as shown in Fig. 7.21B. The strategy of using ferromagnetic micro-concentrator field lines was also demonstrated for the detection of proteins. The concentrators were obtained by patterning thin or thick microstructures made of nickel or permalloy [68, 107–109]. Yu et al. [108] realized a microfluidic device integrating a nickel array that was able to trap magnetic beads in eight parallel channels as shown in Fig. 7.21C. The obtained self-assembled Ab-magnetic bead patterns allowed to simultaneously detecting eight different cancer biomarkers in the eight parallel branches of the device. A more anecdotal method that consists in packing micrometric magnetic beads in microfluidic chamber [110] was also published.

7.5.2.2 Magnetic Bio-Devices for Cell Manipulation

Two approaches are developed to manipulate cells using magnetophoretic forces: label-free approach and the use of magnetic labels on cells.

Label-Free Cell Manipulation

Two strategies are reported to manipulate label-free cells in magnetic bio-devices: manipulation of diamagnetic cells using ferromagnetic fluids and manipulation of cells possessing intrinsic magnetic properties. Manipulation of diamagnetic cells
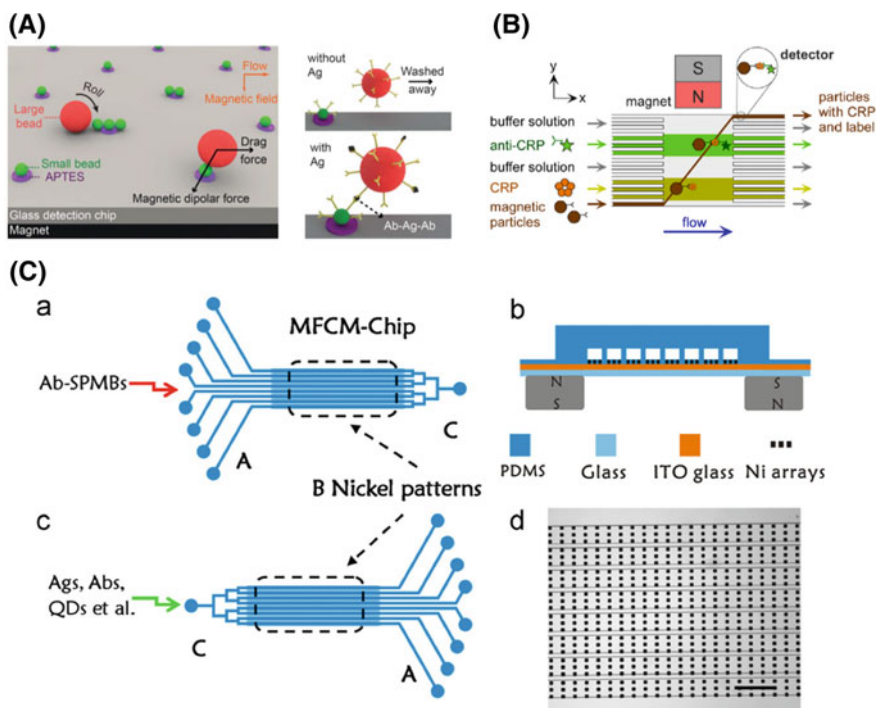
Fig. 7.21 **A** Detection area covered with a small (1.0 mm) bead pattern. Large beads loaded with Ab-Ag immunocomplexes at their surface are transported in this area and roll on the pattern under a magnetic field until they can bind specifically to the small beads by the formation of Ab-Ag-Ab immunocomplexes (Reproduced from [104], with permission of The Royal Society of Chemistry). **B** Principle of the multilaminar flow platform for a CRP sandwich assay: functionalized magnetic particles move through alternating streams of reagents and washing buffers via an external magnet (Reproduced with permission from [106], copyright (2014) American Chemical Society) **C** Schematic of the microfluidic device developed to perform detection of cancer biomarkers using self-assembled magnetic bead patterns. In d, optical image on the nickel pattern array channels (scale bare is 500 μm) (Reproduced from [108], copyright (2013), with permission of Elsevier)

remains challenging, in particular regarding ferrofluids biocompatibility. The reader can find information on this approach in these reviews [4, 111, 112]. In contrast, cells with intrinsic magnetic properties (deoxygenated red blood cells (RBC), and malaria infected RBCs) can be manipulated in bio-devices using standard aqueous buffers.

Red blood cells (RBC) have a paramagnetic behavior when deoxygenated (in veins) and a diamagnetic behavior when oxygenated (in arteries). In RBC vertebrates, hemoglobin is an iron-containing molecule that carries oxygen from the respiratory organs (lungs or gills) to the rest of the body. Oxygenated hemoglobin is diamagnetic due to the presence of paired electrons on its Fe atoms. Deoxyhemoglobin is the form of hemoglobin without the bound oxygen to the Fe

atoms, thus containing four or five unpaired electrons. As a consequence, deoxy-hemoglobin presents a paramagnetic behavior, deoxygenated RBCs have a relative magnetic susceptibility of $\Delta\chi_{deox} = \chi_{deoxRBC} - \chi_{water} = 3.3 \, 10^{-6}$ in water. Although this value is relatively small, it allows exerting sufficient magnetic forces on deox-RBCs in order to trap or separate them from other cells in total blood. This was illustrated by Melville et al. [113] in 1975 and since then, numerous works were published with improvement in the efficiency of RBCs recovery [7–9, 114–118]. For example, Jung et al. [116], developed a microfluidic system with a separation function consisting of six-stages (Fig. 7.22a). This approach allowed separating RBCs from human whole blood sample with a throughput up to 50 μL/h with an efficiency of 86% for RBCs. Each separation stage is a micro-concentrator of magnetic flux of thick ferromagnetic nickel microstructures that allow obtaining magnetic field gradient over the entire channel thickness. A schematic of the device with picture of separation at different stage is shown in Fig. 7.22a.

Besides general blood separation, magnetophoretic forces were used for separation of malaria infected RBCs (iRBCs) in blood. Human malaria is caused by four types of parasites, among which *Plasmodium falciparum* being the most fatal. To prosper in RBCs, malaria parasite needs to clear out hemoglobin which is toxic to them. They convert it in an insoluble crystal known as hemozoin. The ion Fe^{3+} in hemozoin has a stronger paramagnetic character than iron in hemoglobin (Fe^{2+}), and thus increase the infected RBCs magnetic susceptibility relative to water $\left(\Delta\chi = 1.8 \, 10^{-6}\right)$ compared to oxygenated RBC $\left(\Delta\chi = -0.18 \, 10^{-6}\right)$, while remaining lower than deox RBCs [119, 120]. During infection, *P. falciparum* parasite is present at different maturation stages in RBCs, late one being the more paramagnetic. Several works were reported in literature to perform separation of
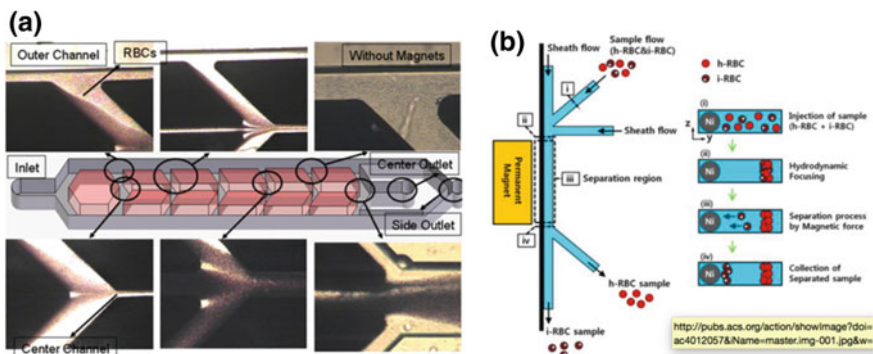
Fig. 7.22 **a** The RBCs are attracted towards ferromagnetic structures through the center channel, while white blood cells WBCs and other rare cells travel along the outer channel. The remaining RBCs in the outer channel are attracted and separated again subsequent separation stages. Micrographs of the blood cell separation at each stage are reported (Reproduced from [116], copyright (2010), with permission of Springer). **b** Schematic diagram of i-RBC separation using the paramagnetic characteristics of hemozoin in i-RBCs (Reproduced with permission from [123], copyright (2013) American Chemical Society)

iRBCs [121–125]. Nam [123] presented a system dedicated to magnetic separation of iRBCs at various stages of maturation (Fig. 7.22b). Their micro-channel possesses three inlets and two outlets. RBCs and i-RBCs mixture was injected in the central inlet, and sheath fluids were injected from the two side inlets. Their role was to focus RBCs at an optimized distance of the nickel wire. RBCs flowed in the channels, and infected ones were attracted toward the nickel wire due to magnetophoretic forces, whereas healthy ones kept flowing along the focus streamline. Using this device, the obtained recovery rate was 99% for late stage i-RBCs et 73% for early ring stage i-RBCs. Notice that, malaria diagnosis in magnetic bio-devices can also be achieved via detection of parasite biomarkers (proteins) present in whole blood, serum and plasma, using functionalized magnetic beads.

Magnetically Labeled Cells

Cells that do not possess intrinsic magnetic properties can be magnetically labeled via two approaches: (i) by internalization into the cytoplasm of nanoparticles (by endositosis [126], phagositosis [127] or transfection [128]) and (ii) by attachment of nanoparticles on their surface. The first approach, in which MNP cross the cell membrane and enter the cytoplasm, is mainly dedicated to enable MRI, drug targeted delivery or to study intracellular process. For the second approach, [129] attachment of NP on the cell membrane can be performed through specific ligand-receptor interaction, such as Ag-Ab, specific lectins or other sugar binding protein, avidin and streptavidin, for example. Other technics can be used to magnetically modify cells. For example by coating MNP on cell membrane using electrostatic interactions, binding of ferritin and magnetoferritin, entrapment of cells into biocompatible magnetic polymers and gels... [129]. Note, that it is generally accepted that attached beads do not modify cells viability, except on sensitive cell population such as stem and progenitor cells [14]. Depending on the labeling approach, the expression of the magnetophoretic force can be adjusted. Either the magnetic cell iron content can be estimated using magnetophoretic method [130], or in the particular case of immunomagnetically labeled cells, the magnetic force can be slightly adapted to depict the tagging of a single cell with numerous smaller magnetic particles [131], as expressed in Eq. (7.38)

$$\overrightarrow{F_{\mathrm{m}}} = \mu_0 V_p \beta j \vartheta \lambda \left(\overrightarrow{M}_p \cdot \overrightarrow{\nabla} \right) \overrightarrow{H} \qquad (7.38)$$

β being the number of nanoparticles conjugated to the targeted Ab, j the number of Ag binding sites per cells, ϑ the fraction of Ag on the cell surface bound by targeted Ab and, λ the valence of the Ab binding, i.e. the number of Ag that binds an anti-body, and V_p, the volume of a MNP.

This expression can be modified to take into account binding of secondary Ab to sites present on the primary Ab [132]. The product $\beta j \vartheta \lambda$, is equivalent to the number of bounded magnetic particles on cells, N, $\overrightarrow{F_m}$ can therefore be written as [65]:

$$\overrightarrow{F_m} = N \overrightarrow{F_P} \tag{7.39}$$

$\overrightarrow{F_P}$ being the force exerted on a single nano-particle.

Sajay et al. [133] proposed the following expression for the magnetic force, considering that magnetic particles are saturated:

$$\overrightarrow{F_m} = \mu_0 V_p \Delta\chi_c \left(\overrightarrow{H} \cdot \overrightarrow{\nabla} \right) \overrightarrow{H} \tag{7.40}$$

$\Delta\chi_c$ being the effective magnetic susceptibility of the cell-particle complex:

$$\Delta\chi_c = N \frac{R_p^3}{R_c^3} \Delta\chi_p \tag{7.41}$$

R_p and R_c being respectively the radius of the nano-particle and the cell, $\Delta\chi_p$, the effective susceptibility of the nano-particle.

One can notice that, the radius of the cell-particle complex must be considered for other forces, such as the drag and the gravitational forces described in Sect. 7.2. The cell-particle complex radius can be approximated by:

$$R = \left(R_c^3 + R_p^3 \right)^{\frac{1}{3}} \tag{7.42}$$

Magnetophoretic manipulation of labelled cells in microfluidic devices are mainly focused on separation of white blood cells (WBCs) [133, 134] from blood sample, bacteria from serum or blood sample [135] and rare circulating cells from blood sample [4, 14, 84, 136]. In particular, enrichment of a target cell population and subsequent culture is an important step in the fields of molecular genetics, proteomics, biology and medicine. Regarding biomedical field, many applications require sorting of rare cells that are defined as cells representing less than 1% of the total number of cells. Among examples, we can cite circulating tumor cells (CTCs), circulating endothelial cells (CEC), endothelial progenitor cells (EPCs). Isolation of rare cells represent a big challenge for diagnostic and monitoring of diseases of strong societal interest such as cancer, cardiovascular disease and prenatal diagnostic. Labeling based on specific attachment of MNPs on the cell membrane, in particular immunomagnetic approach in which a micro- or nano-particles bind to cells through Ab-Ag recognition, suits particularly well this application. This approach is the most widely used in microfluidic systems. At the macroscale, magnetic activated cell sorting (MACS) systems consist in attracting labeled cells

on a tube wall using an external magnetic field whereas unlabeled cells are eluted. Then target cells are released once the external magnetic field is removed. The U.S. Food and Drug Administration (FDA) approved the Veridex system, CellSearch^{TM}. This apparatus is a commercial system based on MACS method used to detect CTCs and currently employed for clinical diagnosis of breast, colorectal and lung cancers. However, this system works only for EpCAM surface marker expression, limiting its capture efficiency. Downscaling MACS allow portability (point-of care diagnosis), and improved control of magnetic and hydrodynamic forces exerted on target cells in order to achieve better separation efficiency. µMACS is widely employed for CTC detection in microfluidic systems [65, 84, 136].

Three parameters allow assessing the efficiency of cell separation: (i) the purity, i.e. the number of target cells among separated cells, (ii) the recovery, i.e. the number of separated cells versus the total number of cells or versus the number of target cells in the original suspension, and (iii) the viability of cells, i.e. subsequent capacity of separated cells to be considered as alive with living cell assay or cell culture. Two approaches are reported to address these challenges, positive enrichment, i.e. capturing labeled CTCs and eluting blood cells, or negative selection, i.e. capture labeled blood cells and eluting CTCs. In the first case, recovery and purity rates are reported to be superior. However, this approach presents some limitations. Because of the heterogeneous nature of target cells, they do not all express the same Ags, and some target cells with unknown surface biomarkers may be excluded from separation. In addition, the removing of MNPs from cell surface can remain challenging, and may damage cells. Indeed, the detachment process can involve saturated protein solutions, enzymes able to cleave beads form the cells, temperature induced method, which are either not efficient for all cells or may diminish cell viability.

µMacs implementing a single external permanent magnet are reported [137–142]. Their interest is to release trapped particles when removing the magnet. However, low magnetophoretic forces are reached due to magnet size and the large distance between the magnetic field gradient and the target objects in the channel. For instance, Kang et al. [139] and Wang et al. [142] proposed two different systems both based on the entrapment of labeled CTCs in a flow where both CTCs and blood cells are present. In presence of the magnetic field gradient, labeled cells were deviated towards specific compartments, and could then be released by removing the magnet. Oskumur et al. [138], combined size based filtration assay, inertial focusing and immuno-magnetic assay for efficient capture of both EpCAM positive and EpCAM negative cancer cells. In a first step, separation of WBCs and CTCs from RBCs and platelets was achieved using deterministic lateral displacement. In a second step, alignment of cells in the micro-channel was obtained using inertial focusing, and finally magnetically labeled cells, either CTCs, or WBCs, were deflected into a collection channel using magnetophoretic forces. The inertial focusing strategy, permitted to obtain the alignment of cells in a near single line, in order to prevent cellular collisions during magnetophoresis and to precisely control their position in the main channel in order to deflect them using minimal magnetic force.

Microsystems integrating an array of millimeter size permanent magnets are also reported [143, 144]. Multiple magnetic field gradients can then be achieved directly in the channel while still allowing the release of trapped particles by removing magnets. For instance, Lee et al. [143] developed a μ-MixMACS chip for CTC isolation using negative selection. It consisted in a mixing module for effective binding between WBCs and MNPs coated with CD45 Ab and a magnetic-activated cell sorting module to capture WBCs inside the channel. This resulted in the depletion of magnetically labeled WBCs. In contrast, CTCs kept flowing in the channel and were recovered in the outlet. As schematically showed in Fig. 7.23a, the bio-device was composed of three superposed channels: a micromixer, an incubation chamber and an enrichment channel. The magnet array comprised 21 NdFeB pieces. They were arrayed in a laser-cut plastic cartridge with 2 mm gap between adjacent magnets with alternating polarity. The authors compared the separation efficiency obtained in their device with a commercially available kit, EasySep[TM] Human CD45 Depletion Kit. They reported better CTCs recovery rate in their microsystem.

Integrated arrays of permanent micron-size magnets were also reported for cell manipulation [44, 145]. They presented the advantage to achieve higher forces thanks to magnet down-scaled down to cell size. However, releasing of trapped cells remains challenging so this approach is more adapted for in channel observation or treatment of cells.

Micro-concentrators of magnetic flux were also largely employed for labeled cells sorting in bio-device, and various methods are reported in literature [135, 146–148]. Ferromagnetic thin film approach is reported in Esmaeilsabzali et al. [146] publication. They proposed a system for detection and isolation of prostate cancer cells from blood. This system featured large trapping surface consisting in V-shaped Permalloy ferromagnetic micro-traps as shown in Fig. 7.23b.

The sample continuously flowed through the channels and labeled cells were deviated towards magnetic microtraps. In order to display magnetophoretic force in the whole channel thickness, thick approaches were also reported. For instance, Malik et al. [135], presented a 3D polymer –based microchip for immuno-magnetic capture and release of *Listeria monocytogenes*. Their device was made of cyclo olefin copolymer (COC) and contained an array of 3D micro-pillars (diameter of 20 μm; height of 67 μm) coated with a layer of nickel. A picture of the bio-device highlighting the integrated pillars, and a schematic of principle are shown in Fig. 7.23c. The fabrication process involving hot-embossing and electroless deposition is compatible with mass-production. In addition, they designed their system in a way that the magnetic field is applied perpendicular to the flow in order to facilitate the release of particles when the magnetic field is removed. It comprised a wide capture chamber, containing the pillars, to process large volumes. Faivre et al. [67] developed an elegant approach based in composite polymer for labeled cell manipulation. They proposed a trapping device using thick composite iron-PDMS (I-PDMS) microstructures to generate large magnetic field gradient. Saliba et al. [148] developed an original method, consisting in an array of column of self-assembled bio-functionnalized superparamagnetic particles, on which target
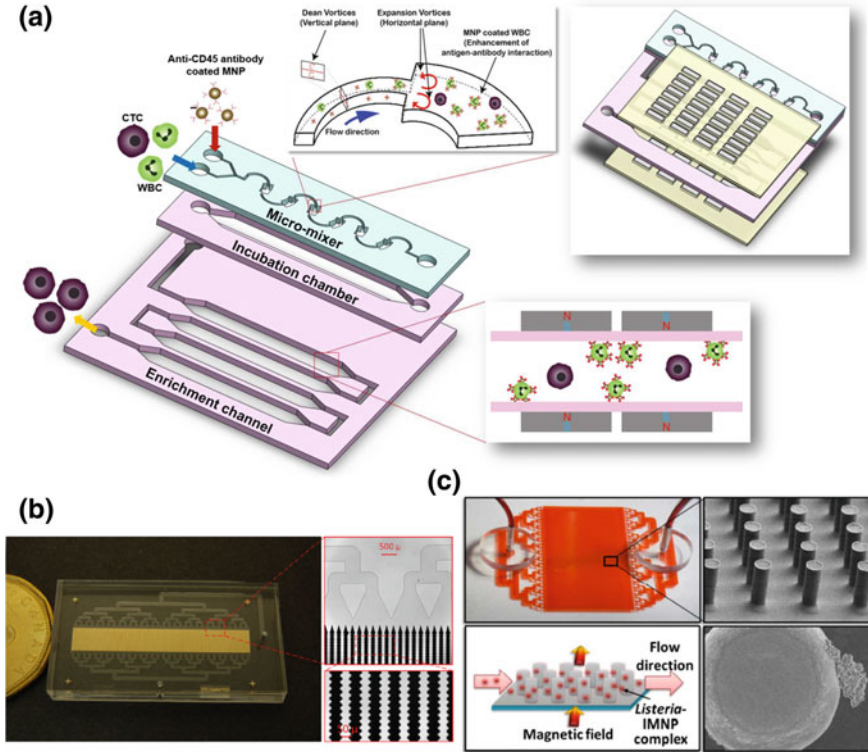
Fig. 7.23 **a** Schematic of a μ-MixMACS chip for one-step CTC isolation using the negative depletion approach. It is composed of three parts: a microfluidic mixer to favor binding between CD45 conjugated MNPs and WBCs, an incubation chamber that permit stable MNP conjugation to the WBCs, and MACS function dedicated to capture the labeled WBCs and elute CTCs through the outlet (Reproduced from [143], copyright (2017), with permission of Elsevier). **b** Photograph of the microchip integrating patterned Permalloy strips. The resulting V-shaped magnetic microtraps seen under microscope are shown (Reproduced from [146], copyright (2016), with permission of Springer). **c** Photograph of 3D polymer-based chip and of the integrated magnetic pillars, and schematic of principle of the device (Reproduced from [135], with permission of The Royal Society of Chemistry)

cells are trapped through Ag-Ab recognition. The substrate was patterned by microcontact printing in order to locally deposit water-based ferrofluid onto glass. These ferromagnetic dots acted as micro-concentrator of magnetic flux in order to assemble magnetic particles in columns. Then, these magnetic particles were functionalized and, via Ag-Ab interaction, cells were trapped on the columns.

7.6   Conclusion

Associating magnetism to microfluidics permit to address numerous challenges for biomedical applications. This combination permit precise manipulation of functionalized micro-particles or biological entities such as magnetically labeled cells or natively paramagnetic RBCs. Indeed, micro- and nano-objects exposed to a non–uniform magnetic field undergo a translational magnetic force referred as magnetophoresis. This force depends on the magnetic nature of the target object and can be greatly increased by integrating micro-sources of magnetic flux directly inside of microfluidic channel. Thus, the magnetic force can predominate, in this environment, over other forces such as drag or gravitational forces. The precise balance of these forces allows describing the motion of target objects and to manipulate them. The implementation of magnetophoretic functions in bio-device are mainly performed using permanent micro-magnet or micro-concentrators of magnetic flux. Both options can lead to comparable maximum force intensities for any given target objects. Permanent micro-magnets do not require any exterior flux to operate, which permits to develop devices with incomparable compactness, but in turns are bound to remain active, with fixed force strength. In contrast, the micro-concentrators of magnetic flux offer easy and real time modulation of the generated force, allowing releasing the trapped object when required. Concerning bio-analysis, magnetic particles present the advantage of versatility in their functionalization. They can thus serve to develop various detection routes, like for nucleic acid and proteins, or for labeling diamagnetic cells, which was notably exploited for blood fractionation, CTCs trapping and sorting. As they do not set restrictions on the target objects, magnetophoretic forces can be easily associated to other forces, dielectrophoresis for instance [149], to improve their separation efficiency.

References

1. M.A.M. Gijs, F. Lacharme, U. Lehmann, Microfluidic applications of magnetic particles for biological analysis and catalysis. Chem. Rev. **110**, 1518–1563 (2010)
2. N. Pamme, On-chip bioanalysis with magnetic particles. Curr. Opin. Chem. Biol. **16**, 436–443 (2012)
3. N. Pamme, J.C.T. Eijkel, A. Manz, On-chip free-flow magnetophoresis: Separation and detection of mixtures of magnetic particles in continuous flow. J. Magn. Magn. Mater. **307**, 237–244 (2006)
4. M. Hejazian, W. Li, N.T. Nguyen, Lab on a chip for continuous-flow magnetic cell separation. Lab Chip (2015). https://doi.org/10.1039/c4lc01422g
5. L. Borlido, A.M. Azevedo, A.C.A. Roque, M.R. Aires-Barros, Magnetic separations in biotechnology. Biotech. Adv. **13**, 1374–1385 (2013)
6. T.P. Forbe, S.P. Forry, Microfluidic magnetophoretic separations of immunomagnetically labeled rare mammalian cells. Lab Chip **12**, 1471 (2012)
7. J. Jung, H.K. Han, Lateral-driven continuous magnetophoretic separation of blood cells. Appl. Phys. Lett. **93**, 223902 (2008)

8. M. Zborowski, G.R. Ostera, L.R. Moore, S. Milliron, J.J. Chalmers, Red blood cell magnetophoresis. Biophys. J. **84**, 2638–2645 (2003)

9. B.Y. Qu, Z.Y. Wu, F. Fang, Z.M. Bai, D.Z. Yang, S.K. Xu, A glass microfluidic chip for continuous blood cell sorting by a magnetic gradient without labeling. Anal. Bioanal. Chem. **392**, 1317–1324 (2008)

10. J. Luo, X. He, D. Andre' d'Avignon, J.J.H. Ackerman, D.A. Yablonskiy, Protein-induced water 1H MR frequency shifts: contributions from magnetic susceptibility and exchange effects. J. Magn. Reson. **202**(1), 102 (2010)

11. M.D. Graham, P.R. Selvin, Separation of lanthanide-binding cells. IEEE T. Magn. **18**(6), 1523 (1982)

12. A.D. Buckingham, T. Schaefer, W.G. Schneider, Solvent effects in nuclear magnetic resonance spectra. J. Chem. Phys. **32**, 1227 (1960)

13. J.M.D. Coey, *Magnetism and Magnetic Materials* (Cambridge University Press, Cambridge, 2010)

14. B.D. Plouffe, S.K. Murthy, L.H. Lewis, Fundamentals and application of magnetic particles in cell isolation and enrichment: a review. Rep. Prog. Phys. **78**(1), 016601 (2015)

15. P. Talagala, P.S. Fodor, D. Haddad, R. Naik, L.E. Wenger, P.P. Vaishnava, V.M. Naik, Determination of magnetic exchange stiffness and surface anisotropy constants in epitaxial $Ni_{1-x}Co_x$(001) films. Phys. Rev. B **66**, 144426 (2002)

16. W. Wu, X.H. Xiao, S.F. Zhang, T.C. Peng, J. Zhou, F. Ren, C.Z. Jiang, Synthesis and magnetic properties of maghemite (gamma-Fe_2O_3) short-nanotubes. Nanoscale Res. Lett. **5**(9), 1474–1479 (2010)

17. E.P. Furlani, Magnetic biotransport: analysis and applications. Materials **3**, 2412–2446 (2010)

18. R. Wirix-Speetjens, W. Fyen, K. Xu, J. De Boeck, G. Borghs, A force study of on-chip magnetic particle transport based on tapered conductors. IEEE T. Magn. **41**, 4128 (2005)

19. X. Han, Y. Feng, Q. Cao, L. Li, Three-dimensional analysis and enhancement of continuous magnetic separation of particles in microfluidics. Microfluid. Nanofluid. (2016). https://doi.org/10.1007/s10404-014-1516-6

20. E.P. Furlani, K.C. Ng, Analytical model of magnetic nanoparticle transport and capture in the microvasculature. Phys. Rev. E **73**, 061919 (2006)

21. Q. Cao, X. Han, L. Li, Configurations and control of magnetic fields for manipulating magnetic particles in microfluidic applications: magnet systems and manipulation mechanisms. Lab Chip (2014). https://doi.org/10.1039/c4lc00367e

22. W. Zhao, R. Cheng, J.R. Miller, L. Mao, Label-free microfluidic manipulation of particles and cells in magnetic liquids. Adv. Funct. Mater. (2016). https://doi.org/10.1002/adfm.201504178

23. R. Zhou, Q. Yang, F. Bai, J.A. Werner, H. Shi, Y. Ma, C. Wang, Microfluid. Nanofluid. **20**, 110 (2016)

24. A. Sinha, R. Ganguly, I.K. Puri, Magnetic separation from superparamagnetic particle suspensions. J. Magn. Magn. Mater. **321**, 2251–2256 (2009)

25. R. Gerber, Magnetic filtration of ultra-fine particles. IEEE T. Magn. **20**, 1159 (1984)

26. R. Gerber, M. Takayasu, F.J. Friedlaender, Generalization of HGMS theory: the capture of ultra-fine particles. IEEE T. Magn. **19**, 2115 (1983)

27. M. Takayasu, R. Gerber, F.J. Friedlaender, Magnetic separation of submicron particles. IEEE T. Magn. **19**, 2112 (1983)

28. D. Fletcher, Fine particle high gradient magnetic entrapment. IEEE T. Magn. **27**, 3655 (1991)

29. E.P. Furlani, K.C. Ng, Nanoscale magnetic biotransport with application to magnetofection. Phys. Rev. E **77**, 061914 (2008)

30. A. Sinha, R. Ganguly, A.K. De, I.K. Puri, Single magnetic particle dynamics in a microchannel. Phys. Fluids **19**, 117102 (2007)

31. K. Nandy, S. Chaudhuri, R. Ganguly, I.K. Puri, Analytical model for the magnetophoretic capture of magnetic microspheres in microfluidic devices. J. Magn. Magn. Mater. **320**, 1398–1405 (2008)
32. R. Fulcrand, A. Bancaud, C. Escriba, Q. He, S. Charlot, A. Boukabache, A.M. Gué, On chip magnetic actuator for batch-mode dynamic manipulation of magnetic particles in compact lab-on-chip. Sens. Actuat. B Chem. **160**(1), 1520–1528 (2011)
33. P.T. Tseng, D. Di Carlo, J.W. Judy, Rapid and dynamic intracellular patterning of cell-internalized magnetic fluorescent nanoparticles. Nano Lett. **9**(8), 3053–3059 (2009)
34. L. Zanini, N.M. Dempsey, D. Givord, G. Reyne, F. Dumas-Bouchiat, Autonomous micro-magnet based systems for highly efficient magnetic separation. Appl. Phys. Lett. **99**, 232504 (2011)
35. N.M. Dempsey, in *Nanoscale Magnetic Materials and Applications*, ed. by J.P. Liu, E. Fullerton, O. Gutfleisch, D.J. Sellmyer (Springer, New York, 2009), pp. 661–680
36. A. Beyzavi, N.T. Nguyen, Modeling and optimization of planar microcoils. J. Micromech. Microeng. **18**, 095018 (2008)
37. R. Fulcrand, D. Jugieu, C. Escriba, A. Bancaud, D. Bourrier, A. Boukabache, A.M. Gué, Development of a flexible microfluidic system integrating magnetic micro-actuators for trapping biological species. J. Micromech. Microeng. **19**, 105019 (2009)
38. K. Yamauchi, J.W.G. Janssen, A.P.M. Kentgens, Implementing solenoid microcoils for wide-line solid-state NMR. J. Magn. Reson. **167**, 87–96 (2004)
39. A. Haase, F. Odoj, M. Von Kienlin, J. Warnking, F. Fidler, A. Weisser, M. Nittka, E. Rommel, T. Lanz, B. Kalusche, M. Griswold, NMR probeheads for in vivo applications. Concept Magn. Reson. A **12**(6), 361–388 (2000)
40. K. Kamata, Z. Piao, S. Suzuki, T. Fujimori, W. Tajiri, K. Nagai, T. Iyoda, A. Yamada, T. Hayakawa, M. Ishiwara, S. Horaguchi, A. Belay, T. Tanaka, K. Takano, M. Hangyo, Spirulina-templated metal microcoils with controlled helical structures for THz electromagnetic responses. Sci. Rep. **4**, 4919 (2014)
41. J.M.D. Coey, New permanent magnets; manganese compounds. J. Phys. Condens. Mat. **26**, 064211 (2014)
42. J.M.D. Coey, Hard magnetic materials: a perspective. IEEE T. Magn. **47**, 12 (2011)
43. R. Engel-Hebert, T. Hesjedal, Calculation of the magnetic stray field of a uniaxial magnetic domain. J. Appl. Phys. **97**, 074504 (2005)
44. V. Zlabotskii, A. Dejneka, S. Kubinova, D. Le Roy, F. Dumas-Bouchiat, D. Givord, N.M. Dempsey, E. Sykova, Life on magnets: stem cell networking on micro-magnet arrays. PLoS ONE **8**(8), e70416 (2013)
45. M. Nakano, K. Yamaguchi, T. Yanai, F. Yamashita, H. Fukunaga, Change in the direction of anisotropy in PLD-fabricated Sm-Co thick film magnets. J. Appl. Phys. **105**, 7 (2009)
46. F. Ruiyi, F. Qingqing, Z. Sheng, P. Chubing, D. Daosheng, New permanent magnetic MnBiDy alloy films. J. Appl. Phys. **76**, 10 (1994)
47. F.M. Rhen, G. Hinds, C. O'Reilly, J.M.D. Coey, Electrodeposited FePt films. IEEE T. Magn. **39**, 5 (2003)
48. N.M. Dempsey, A. Walther, F. May, D. Givord, K. Khlopkov, O. Gutfleisch, High performance hard magnetic NdFeB thick films for integration into micro-electro-mechanical systems. Appl. Phys. Lett. **90**, 092509 (2007)
49. C. Delcour, G. Bugnicourt, N.M. Dempsey, F. Dumas-Bouchiat, C. Villard, Combined magnetic and chemical patterning for neural architectures. J. Phys. D Appl. Phys. **47**, 425403 (2014)
50. A. Walther, C. Marcoux, B. Desloges, R. Grechishkin, D. Givord, N.M. Dempsey, Micro-patterning of NdFeB and SmCo magnet films for integration into micro-electro-mechanical-systems. J. Magn. Magn. Mater. **321**, 590–594 (2008)
51. T. Okuda, A. Sugimura, O. Eryu, L.K.E.B. Serrona, N. Adachi, I. Sakamoto, A. Nakanishi, Nd-Fe-B thin films with perpendicular magnetic anisotropy and high coercivity prepared by pulsed laser annealing. Jpn. J. Appl. Phys. **42**, 6859–6864 (2003)

52. J. Topfer, B. Pawlowski, H. Beer, K. Plotner, P. Hofmann, J. Herrfurth, Multi-pole magnetization of NdFeB magnets for magnetic micro-actuators and its characterization with a magnetic field mapping device. J. Magn. Magn. Mater. **270**, 124–129 (2004)
53. J. Topfer, V. Christoph, Multi-pole magnetization of NdFeB sintered magnets and thick films for magnetic micro-actuators. Sens. Actuat. A Phys. **113**, 257–263 (2004)
54. F. Dumas-Bouchiat, L. Zanini, M. Kustov, N.M. Dempsey, R. Grechishkin, K. Hasselbach, J.C. Orlianges, C. Champeaux, A. Catherinot, D. Givord, Thermomagnetically patterned micromagnets. Appl. Phys. Lett. **96**, 102511 (2010)
55. O.D. Oniku, P.V. Ryiz, A. Garraud, D.P. Arnold, Imprinting of fine-scale magnetic patterns in electroplated hard magnetic films using magnetic foil masks. J. Appl. Phys. **115**, 17A718 (2014)
56. D. Le Roy, G. Shaw, R. Haettel, K. Hasselbach, F. Dumas-Bouchiat, D. Givord, N.M. Dempsey, Fabrication and characterization of polymer membranes with integrated arrays of high performance micro-magnets. Mater. Today Commun. **6**, 50–55 (2016)
57. M. Pallapa, J.T.W. Yeow, A review of hybrid techniques for the fabrication of hard magnetic microactuators based on bonded magnetic powder. Smart Mater. Struct. **24**, 025007 (2015)
58. O.D. Oniku, B.J. Bowers, S.B. Shetye, N. Wang, D.P. Arnold, Permanent magnet microstructures using dry-pressed magnetic powders. J. Micromech. Microeng. **23**, 075027 (2013)
59. N.M. Dempsey, D. Le Roy, H. Marelli-Mathevon, G. Shaw, A. Dias, R.G.B. Kramer, M. Le Viet Cuong Kustov, L. Zanini, C. Villard, K. Hasselbach, C. Tomba, F. Dumas-Bouchiat, Micro-magnetic imprinting of high gradient magnetic flux sources. Appl. Phys. Lett. **104** (26), 262401 (2014)
60. C. Velez, I. Torres-Diaz, L. Maldonado-Camargo, C. Rinaldi, D. Arnold, Magnetic assembly and cross-linking of nanoparticles for releasable magnetic microstructures. ACS Nano **9**(10), 10165–10172 (2015)
61. G. Shaw, R.G.B. Kramer, N.M. Demspey, K. Hasselbach, A scanning hall probe microscope for high resolution, large area, variable height magnetic field imaging. Rev. Sci. Instrum. **87** (11), 113702 (2016)
62. B.D. Cullity, C.D. Graham, *Introduction to Magnetic Materials*, 2nd edn. (Wiley-IEEE press, Piscataway, 2008)
63. O. Gutfleisch, M.A. Willard, E. Bruck, C.H. Chen, S.G. Sankar, J.P. Liu, Magnetic materials and devices for the 21st century: stronger, lighter, and more energy efficient. Adv. Mater. **23**, 821–842 (2011)
64. J.A. Osborn, Demagnetizing factors of the general ellipsoid. Phys. Rev. **67**, 11 (1945)
65. P. Chen, Y.Y. Huang, K. Hoshino, X. Zhang, Multiscale immunomagnetic enrichment of circulating tumor cells: from tubes to microchips. Lab Chip **14**, 446 (2014)
66. T. Deng, M. Prentiss, G.M. Whitesides, Fabrication of magnetic microfiltration systems using soft lithography. Appl. Phys. Lett. **80**(3), 461 (2002)
67. F. Faivre, R. Gelszinnis, J. Degouttes, N. Terrier, C. Riviere, R. Ferrigno, A.L. Deman, Magnetophoretic manipulation in microsystem using carbonyl iron-polydimethylsiloxane microstructures. Biomicrofluidics **8**, 054103 (2014)
68. M. Abonnenc, A.L. Gassner, J. Morandini, J. Josserand, H.H. Girault, Magnetic track array for efficient bead capture in microchannels. Anal. Bioanal. Chem. **395**, 747–757 (2009)
69. P. Chen, Y.Y. Huang, G. Bhave, K. Hoshino, X. Zhang, Inkjet-Print micromagnet array on glass slides for immunomagnetic enrichment of circulating tumor cells. Ann. Biomed. Eng. **44**(5), 1710–1720 (2016)
70. D. Le Roy, D. Dhungana, L. Ourry, M. Faivre, R. Ferrigno, A. Tamion, V. Dupuis, V. Salles, A.L. Deman, Anisotropic ferromagnetic polymer: a first step for their implementation in microfluidic systems. AIP Adv. **6**(5), 056604 (2016)
71. C.C. Berry, A.S.G. Curtis, Functionalisation of magnetic nanoparticles for applications in biomedicine. J. Phys. D Appl. Phys. **36**, R198 (2003)
72. Q.A. Pankhurst, J. Connolly, S.K. Jones, J. Dobson, Applications of magnetic nanoparticles in biomedicine. J. Phys. D Appl. Phys. **36**, R167 (2003)

73. A. Singh, S.K. Sahoo, Magnetic nanoparticles: a novel platform for cancer theranostics. Drug Discov. Today **19**(4), 474–481 (2014)

74. E. Agostinelli, F. Vianello, G. Magliulo, T. Thomas, T.J. Thomas, Nanoparticle strategies for cancer therapeutics: nucleic acids, polyamines, bovine serum amine oxidase and iron oxide nanoparticles. Int. J. Oncol. **46**(5), 16 (2015)

75. J.K. Oh, J.M. Park, Iron oxide-based superparamagnetic polymeric nanomaterials: design, preparation, and biomedical application. Prog. Polym. Sci. **36**, 168–189 (2011)

76. S.C.N. Tang, I.M.C. Lo, Magnetic nanoparticles: essential factors for sustainable environmental applications. Water Res. **47**, 2613–2632 (2013)

77. R.B. Dominguez, G.A. Alonso, R. Muños, A. Hayat, J.L. Marty, Design of a novel magnetic particles based electrochemical biosensor for organophosphate insecticide detection in flow injection analysis. Sens. Actuat. B Chem. **208**, 491 (2015)

78. X. Qu, P.J.J. Alvarez, Q. Li, Applications of nanotechnology in water and wastewater treatment. Water Res. **47**, 3931–3946 (2013)

79. M. Wierucka, M. Biziuk, Application of magnetic nanoparticles for magnetic solid-phase extraction in preparing biological, environmental and food samples. TRAC-Trend. Anal. Chem. **59**, 50–58 (2014)

80. T. Jamshaid, R.T.T. Neto, M. Eissa, N. Zine, M.H. Kunita, A.E. El-Salhi, A. Elaissari, Magnetic particles: from preparation to lab-on-a-chip, biosensors, microsystems and microfluidics applications. TRAC-Trend. Anal. Chem. **79**, 344–362 (2016)

81. J.C. Jokerst, J.M. Emory, C.S. Henry, Advances in microfluidics for environmental analysis. Analyst **137**, 24 (2012)

82. Q. Ramadan, M.A.M. Gijs, Microfluidic applications of functionalized magnetic particles for environmental analysis: focus on waterborne pathogen detection. Microfluid. Nanofluid. **13**, 529–542 (2012)

83. J.H. Kang, J.K. Park, Magnetophoretic continuous purification of single-walled carbon nanotubes from catalytic impurities in a microfluidic device. Small **3**(10), 1784–1791 (2007)

84. Y. Zhu, K. Kekalo, C.N. Dong, Y.Y. Huang, F. Schubitidze, K.E. Griwold, I. Baker, J.X. J. Zhang, Magnetic-nanoparticle-based immunoassays-on-chip: materials synthesis, surface functionalization, and cancer cell screening. Adv. Funct. Mater. (2016). https://doi.org/10.1002/adfm.201504176

85. D.L. Leslie-Pelecky, R.D. Rieke, Magnetic properties of nanostructured materials. Chem. Mater. **8**, 1770–1783 (1996)

86. H. Lee, T.H. Shin, J. Cheon, R. Weissleder, Recent developments in magnetic diagnostic systems. Chem. Rev. **115**, 10690–10724 (2015)

87. A.H. Lu, E.L. Salabas, F. Schüth, Magnetic nanoparticles: synthesis, protection, functionalization, and application. Angew. Chem. Int. Ed. **46**, 1222–1244 (2007)

88. L.H. Reddy, J.L. Arias, J. Nicolas, P. Couvreur, Magnetic nanoparticles: design and characterization, toxicity and biocompatibility, pharmaceutical and biomedical applications. Chem. Rev. **112**, 5818–5878 (2012)

89. S. Laurent, D. Forge, M. Port, A. Roch, C. Robic, L. Vander Elst, R.N. Muller, Magnetic iron oxide nanoparticles: synthesis, stabilization, vectorization, physicochemical characterizations, and biological applications. Chem. Rev. **108**, 2064–2110 (2008)

90. D. Horak, M. Babic, H. Mackova, M.J. Benes, Preparation and properties of magnetic nano-and microsized particles for biological and environmental separations. J. Sep. Sci. **30**, 1751–1772 (2007)

91. J. Kim, M. Johnson, P. Hill, B.K. Gale, Microfluidic sample preparation: cell lysis and nucleic acid purification. Integr. Biol. **1**, 574–586 (2009)

92. P. Liu, X. Li, S.A. Greenspoon, J.R. Scherer, R.A. Mathies, Integrated DNA purification, PCR, sample cleanup, and capillary electrophoresis microchip for forensic human identification. Lab Chip **11**, 1041 (2011)

93. O. Strohmeier, A. Emperle, G. Roth, D. Mark, R. Zengerle, F. von Stetten, Centrifugal gas-phase transition magnetophoresis (GTM) – a generic method for automation of magnetic bead based assays on the centrifugal microfluidic platform and application to DNA purification. Lab Chip **13**, 146–155 (2013)

94. S. Park, Y. Zhang, S. Lin, T.H. Wang, S. Yang, Advances in microfluidic PCR for point-of-care infectious disease diagnostics. Biotechnol. Adv. **29**, 830–839 (2011)

95. Y. Zhang, H.-R. Jiang, A review on continuous-flow microfluidic PCR in droplets: advances, challenges and future. Anal. Chim. Acta (2016). https://doi.org/10.1016/j.aca.2016.02.006

96. T. Kokalj, E. Pérez-Tuiz, J. Lammertyn, Building bio-assays with magnetic particles on a digital microfluidic platform. New Biotechnol. (2015). https://doi.org/10.1016/j.nbt.2015.03.007

97. M. Kühnemund, D. Witters, M. Nilsson, J. Lammertyn, Circle-to-circle amplification on a digital microfluidic chip for amplified single molecule detection. Lab Chip (2014). https://doi.org/10.1039/c4lc00348a

98. P.Y. Hung, P.S. Jiang, E.S. Lee, S.K. Fan, Y.W. Lu, Genomic DNA extraction from whole blood using a digital microfluidic (DMF) platform with magnetic beads. Mycrosyst. Technol. (2015). https://doi.org/10.1007/s00542-015-2512-9

99. G. Czilwik, T. Messinger, O. Strohmeier, S. Wadle, F. von Stetten, N. Paust, G. Roth, R. Zengerle, P. Saarinen, K. Nittymäki, K. McAllister, O. Sheils, J.O. Leary, D. Mark, Rapid molecular infectious disease diagnostics on a fully automated centrifugal-microfluidic LabDisk system using highly sensitive nested PCR with integrated sample preparation. Lab Chip **15**, 3749–3759 (2015)

100. N. Vergauwe, S. Vermeir, J.B. Wacker, F. Ceyssens, M. Cornaglia, R. Puers, M.A.M. Gijs, J. Lammertyn, D. Witters, A highly efficient extraction protocol for magnetic particles on a digital microfluidic chip. Sens. Actuat. B Chem. **196**, 282–291 (2014)

101. X. Lou, J. Qian, Y. Xiao, A.E. Gerdon, E.T. Lagally, P. Atzberger, T.M. Tarasow, A. J. Heeger, H.T. Soh, Micromagnetic selection of aptamers in microfluidic channels. P. Natl. Acad. Sci. USA **106**, 2989–2994 (2009)

102. H.C. Tekin, M.A.M. Gijs, Ultrasensitive protein detection: a case for microfluidic magnetic bead-based assays. Lab Chip (2013). https://doi.org/10.1039/c3lc50477h

103. Y.K. Hahn, J.K. Park, Versatile immunoassays based on isomagnetophoresis. Lab Chip **11**, 2045 (2011)

104. H.C. Tekin, M. Cornaglia, M.A.M. Gijs, Attomolar protein detection using a magnetic bead surface coverage assay. Lab Chip **13**, 1053 (2013)

105. L.A. Sasso, I.H. Johnston, M. Zheng, R.K. Gupte, A. Undar, J.D. Zahn, Automated microfluidic processing platform for multiplexed magnetic bead immunoassays. Microfluid. Nanofluid. **13**, 603–612 (2012)

106. C. Phurimsak, M.D. Tarn, S.A. Peyman, J. Greenman, N. Pamme, On-chip determination of C-reactive protein using magnetic particles in continuous flow. Anal. Chem. **86**, 10552–10559 (2014)

107. J.D. Adams, U. Kim, H.T. Soh, Multitarget magnetic activated cell sorter. P. Natl. Acad. Sci. USA **105**, 18165–18170 (2008)

108. X. Yu, H.S. Xia, A.D. Sun, Y. Lin, K. Wang, J. Yu, H. Tang, D.W. Pang, Z.L. Zhang, On-chip dual detection of cancer biomarkers directly in serum based on self-assembled magnetic bead patterns and quantum dots. Biosens. Bioelectron. **41**, 129–136 (2013)

109. E. Mirowski, J. Moreland, S.E. Russek, M.J. Donahue, Manipulation of magnetic particles by patterned arrays of magnetic spin-valve traps. Appl. Phys. Lett. **84**, 1786 (2007)

110. B. Teste, F. Mallogi, A.L. Gassner, T. Georgelin, J.M. Siaugue, A. Varenne, H. Gurault, S. Descroix, Magnetic core shell nanoparticles trapping in a microdevice generating high magnetic gradient. Lab Chip **11**, 833 (2011)

111. P. Kauffmann, A. Ith, D. O'Brien, V. Gaude, F. Boué, S. Combe, F. Bruckert, B. Schaack, N.M. Dempsey, V. Haguetb, G. Reyne, Diamagnetically trapped arrays of living cells above micromagnets. Lab Chip (2011). https://doi.org/10.1039/c1lc20232d

112. R.J. Yang, H.H. Hou, Y.N. Wang, L.M. Fu, Micro-magnetofluidics in microfluidic systems: a review. Sens. Actuat. B Chem. **224**, 1–15 (2006)

113. D. Melville, F. Paul, S. Roath, Direct magnetic separation of red cells from whole blood. Nature **255**, 706 (1975)

114. K.H. Han, A.B. Frazier, Continuous magnetophoretic separation of blood cells in microdevice format. J. Appl. Phys. **96**, 5797–5802 (2004)

115. K.H. Han, A.B. Frazier, Paramagnetic capture mode magnetophoretic microseparator for high efficiency blood cell separations. Lab Chip **6**, 265–273 (2006)

116. J. Jung, Y. Choi, K.H. Han, A.B. Frazier, Six-stage cascade paramagnetic mode magnetophoretic separation system for human blood samples. Biomed. Microdevices **12**, 637–645 (2010)

117. J.D. Chen, D. Chen, T. Yuan, Y. Xie, X. Chen, A microfluidic chip for direct and rapid trapping of white blood cells from whole blood. Biomicrofluidics **7**, 034106 (2013)

118. L.R. Moore, F. Nehl, J. Dorn, J.J. Chalmers, M. Zborowski, Open gradient magnetic red blood cell sorter evaluation on model cell mixtures. IEEE T. Magn. **49**, 309–315 (2013)

119. S. Hackett, J. Hamzah, T.M.E. Davis, T.G. St Pierre, Magnetic susceptibility of iron in malaria-infected red blood cells. Biochim. Biophys. Acta **1792**, 93–99 (2009)

120. L.R. Moore, H. Fujioka, P.S. Williams, J.J. Chalmers, B. Grimberg, P.A. Zimmerman, M. Zborowski, Hemoglobin degradation in malaria-infected erythrocytes determined from live cell magnetophoresis. FASEB J. **20**, 747–749 (2006)

121. C. Ribaut, A. Berry, S. Chevalley, K. Reybier, I. Molais, D. Parzy, F. Nepveu, F. Benoit-Vical, A. Valentin, Concentration and purification by magnetic separation of the erythrocytic stages of all human plasmodium species. Malaria J. **7**, 45 (2008)

122. S.C. Bhakdi, A. Ottinger, S. Somsri, P. Statongno, P. Pannadaporn, P. Chimma, P. Malasit, K. Pattanapanyasat, H.P.H. Neumann, Optimized high gradient magnetic separation for isolation of plasmodium-infected red blood cells. Malaria J. **9**, 38 (2010)

123. J. Nam, H. Huang, H. Lim, C. Lim, S. Shin, Magnetic separation of malaria-infected red blood cells in various developmental stages. Anal. Chem. **85**, 7316–7323 (2013)

124. W.T. Wu, A.B. Martin, A. Gandini, N. Aubry, M. Massoudi, J.F. Antaki, Design of microfluidic channels for magnetic separation of malaria–infected red blood cells. Microfluid. Nanofluid. **20**, 41 (2016)

125. M. de Souza Castilho, T. Laube, H. Yamanaka, S. Alegret, M.I. Pividori, Magneto immunoassays for plasmodium falciparum histidine-rich protein 2 related to malaria based on magnetic nanoparticles. Anal. Chem. **83**, 5570–5577 (2011)

126. A.T. Jones, M. Gumbleton, R. Duncan, Understanding endocytic pathways and intracellular trafficking: a prerequisite for effective design of advanced drug delivery systems. Adv. Drug Deliv. Reviews **55**, 1353–1357 (2003)

127. S. Marion, C. Wilhelm, H. Voigt, J.C. Bacri, N. Guillén, Overexpression of myosin IB in living *Entamoeba histolytica* enhances cytoplasm viscosity and reduces phagocytosis. J. Cell Sci. **117**(15), 3271–3279 (2004)

128. K. Montet-Abou, X. Montet, R. Weissleder, L. Josephson, Cell internalization of magnetic nanoparticles using transfection agents. Mol. Imaging **6**(1), 1 (2007)

129. I. Safarik, K. Pospiskova, E. Baldikova, Z. Maderova, M. Safarikova, in *Engineering of nanobiomaterials*, ed. by A. Grumezescu (Elsevier, Oxford, 2016), pp. 145–180

130. C. Wilhelm, F. Gazeau, J.C. Bacri, Magnetophoresis and ferromagnetic resonance of magnetically labeled cells. Eur. Biophys. J. **31**, 118 (2002)

131. K.E. McCloskey, J.J. Chalmers, M. Zborowski, Magnetic cell separation: characterization of magnetophoretic mobility. Anal. Chem. **75**, 6868–6874 (2003)

132. K.E. McCloskey, K. Comella, J.J. Chalmers, S. Margel, M. Zborowski, Mobility measurements of immunomagnetically labeled cells allow quantification of secondary antibody binding amplification. Biotechnol. Bioeng. **75**, 642–655 (2001)

133. B.N.G. Sajay, C.P. Chang, P.D. Puiu, Microfluidic immunomagnetic cell separation from whole blood. J. Chromatogr. B **1011**, 77–88 (2016)

134. D.W. Inglis, R. Riehn, R.H. Austin, J.C. Sturm, Continuous microfluidic immunomagnetic cell separation. Appl. Phys. Lett. **85**, 21 (2004)
135. L. Malic, X. Zhang, D. Brassard, L. Clime, J. Daoud, C. Luebbert, V. Barrere, A. Boutin, S. Bidawid, J. Farber, N. Corneau, T. Veres, Polymer-based microfluidic chip for rapid and efficient immunomagnetic capture and release of Listeria monocytogenes. Lab Chip **15**, 3994–4007 (2015)
136. J.H. Myung, S. Hong, Microfluidic devices to enrich and isolate circulating tumor cells. Lab Chip **15**, 4500 (2015)
137. Y.Y. Huang, K. Hoshino, P. Chen, C.H. Wu, N. Lane, M. Huebschman, H.Y. Liu, K. Sokolov, J.W. Uhr, E.P. Frenkel, J.X.J. Zhang, Immunomagnetic nanoscreening of circulating tumor cells with a motion controlled microfluidic system. Biomed. Microdev. **15**, 673 (2013)
138. E. Ozkumur, A.M. Shah, J.C. Ciciliano, B.L. Emmink, D.T. Miyamoto, E. Brachtel, M. Yu, P.I. Chen, B. Morgan, J. Trautwein, A. Kimura, S. Sengupta, S.L. Stott, N.M. Karabacak, T. A. Barber, J.R. Walsh, K. Smith, P.S. Spuhler, J.P. Sullivan, R.J. Lee, D.T. Ting, X. Luo, A. T. Shaw, A. Bardia, L.V. Sequist, D.N. Louis, S. Maheswaran, R. Kapur, D.A. Haber, M. Toner, Inertial focusing for tumor antigen–dependent and –independent sorting of rare circulating tumor cells. Sci. Transl. Med. **5**, 179ra147 (2013)
139. J.H. Kang, S. Krause, H. Tobin, A. Mammoto, M. Kanapathipillai, D.E. Ingber, A combined micromagnetic-microfluidic device for rapid capture and culture of rare circulating tumor cells. Lab Chip **12**, 2175–2181 (2012)
140. J. Kim, U. Steinfeld, H.H. Lee, H. Seidel, Development of a novel micro immune-magnetophoresis cell sorter, in *The 6th Annual IEEE Conference on SENSORS*, 28–31 October (Atlanta, 2007), p. 1081
141. M. Zborowski, J.J. Chalmers, Rare cell separation and analysis by magnetic sorting. Anal. Chem. **83**, 8050–8056 (2011)
142. Z. Wang, W. Wu, Z. Wang, Y. Tang, Y. Deng, L. Xu, J. Tian, Q. Shi, Ex vivo expansion of circulating lung tumor cells based on one-step microfluidics-based immunomagnetic isolation. Analyst (2016). https://doi.org/10.1039/c5an02554k
143. T.Y. Lee, K.A. Hyun, S.I. Kim, H.I. Jung, An integrated microfluidic chip for one-step isolation of circulating tumor cells. Sens. Actuat. B Chem. **238**, 1144–1150 (2017)
144. R.M. Mohamadi, J.D. Besant, A. Mepham, B. Green, L. Mahmoudian, T. Gibbs, I. Ivanov, A. Malvea, J. Stojcic, A.L. Allan, L.E. Lowes, E.H. Sargent, R.K. Nam, S.O. Kelley, Nanoparticle-mediated binning and profiling of heterogeneous circulating tumor cell subpopulations. Angew. Chem. Int. Ed. **53**, 1–6 (2014)
145. O. Osman, L.F. Zanini, M. Frénéa-Robin, F. Dumas-Bouchiat, N.M. Dempsey, G. Reyne, F. Buret, N. Haddour, Monitoring the endocytosis of magnetic nanoparticles by cells using permanent micro-flux sources. Biomed. Microdevices (2012). https://doi.org/10.1007/s10544-012-9673-4
146. H. Esmaeilsabzali, T.V. Beischlag, M.E. Cox, N. Dechev, A.M. Parameswaran, A.J. Park, An integrated microfluidic chip for immunomagnetic detection and isolation of rare prostate cancer cells from blood. Biomed. Microdevices **18**, 22 (2016)
147. T. Dong, Q. Su, Z. Yang, Y. Zhang, E.B. Egeland, D. D. GY, P. Calabrese, M.J. Kapiris, F. Karlsen, N.T. Minh, K. Wang, H. Jakobsen, A smart fully integrated micromachined separator with soft magnetic micro-pillar arrays for cell isolation. J. Micromech. Microeng. **20**, 115021 (2010)
148. A.-E. Saliba, L. Saias, E. Psychari, N. Minc, D. Simon, F.-C. Bidard, C. Mathiot, J.-Y. Pierga, V. Fraisier, J. Salamero, V. Saada, F. Farace, P. Vielh, L. Malaquin, J.-L. Viovy, Microfluidic sorting and multimodal typing of cancer cells in self-assembled magnetic arrays. P. Natl. Acad. Sci. USA **107**(33), 14524–14529 (2010)
149. J. Jung, S.-K. Seo, Y.-D. Joo, K.-H. Han, Label-free continuous lateral magneto-dielectrophoretic microseparators for highly efficient enrichment of circulating nucleated cells from peripheral blood. Sens. Actuat. B Chem. **157**, 314–320 (2011)